

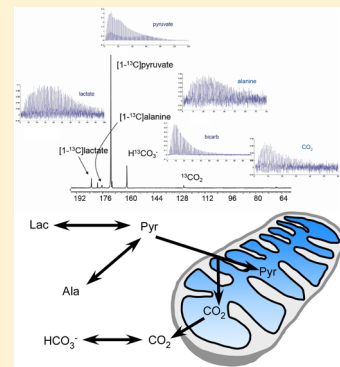
# Hyperpolarized Magnetic Resonance as a Sensitive Detector of Metabolic Function

Arnaud Comment\*,† and Matthew E. Merritt\*,‡

†Institute of Physics of Biological Systems, Ecole Polytechnique Fédérale de Lausanne, CH-1015 Lausanne, Switzerland

‡Advanced Imaging Research Center, Department of Radiology, University of Texas Southwestern Medical Center, Dallas, Texas 75390, United States

**ABSTRACT:** Hyperpolarized magnetic resonance allows for noninvasive measurements of biochemical reactions *in vivo*. Although this technique provides a unique tool for assaying enzymatic activities in intact organs, the scope of its application is still elusive for the wider scientific community. The purpose of this review is to provide key principles and parameters to guide the researcher interested in adopting this technology to address a biochemical, biomedical, or medical issue. It is presented in the form of a compendium containing the underlying essential physical concepts as well as suggestions to help assess the potential of the technique within the framework of specific research environments. Explicit examples are used to illustrate the power as well as the limitations of hyperpolarized magnetic resonance.



Magnetic resonance (MR) has historically been characterized by outstanding chemical selectivity and poor sensitivity. MR imaging (MRI) can be performed at relatively high spatial resolution only because of the large abundance of water protons being imaged, on the order of 80 M in the human body. The wealth of biological and biochemical information characterizing the state of living tissues is however hidden because of the low concentration of the other chemical species, a few millimolar for the largest pools but typically of submillimolar levels. An additional limitation associated with *in vivo* measurements of non-water proton resonances is the low spectral resolution characteristic of <sup>1</sup>H MR spectroscopy (MRS), making it difficult to separate the various metabolites and requiring the necessary and sometimes delicate suppression of the inherently large water signal. This spectroscopic problem can be partly solved by detecting the <sup>13</sup>C resonances of metabolites. <sup>13</sup>C has a low natural isotopic abundance of 1.1%, which means that besides a few compounds such as lipids and glycogen, *in vivo* <sup>13</sup>C signals are detectable only with increased isotopic enrichment. However, the absence of a background signal allows quantitative measurements of the incorporation of <sup>13</sup>C-labeled substrates and their metabolites, thereby allowing specific metabolic pathways to be studied using selective isotopic labeling. Many <sup>13</sup>C MRS metabolic studies have been performed *in vivo* following the injection of substrates such as [<sup>13</sup>C]glucose in animal models and humans.<sup>1–5</sup> However, the lower abundance of <sup>13</sup>C together with its ~4-fold lower gyromagnetic ratio compared to that of <sup>1</sup>H makes the issue of poor sensitivity even more pronounced. <sup>13</sup>C MRS metabolic studies are thus limited to measuring the most abundant amino acids such as glutamate, glutamine, and aspartate in relatively large tissue volumes with low temporal resolution (~5 min in a

state-of-the-art cerebral metabolic study performed *in vivo* in rats at 14.1 T<sup>6</sup>). This implies that numerous metabolic intermediates between the injected <sup>13</sup>C-labeled precursor and the detected metabolites are invisible, and many assumptions are required to derive the underlying enzymatic fluxes.<sup>7–9</sup>

The recent development of hyperpolarization schemes to enhance the <sup>13</sup>C signal by several orders of magnitude allows observing metabolic processes with much higher spatial and temporal resolution than what can be done with thermally polarized <sup>13</sup>C substrates. It also gives access to many intermediates in various metabolic pathways that would otherwise be undetectable. Three schemes have so far been developed to provide hyperpolarized (HP) <sup>13</sup>C metabolic precursors dissolved in room-temperature aqueous solutions: the brute force method, parahydrogen-induced polarization (PHIP), and a method based on dynamic nuclear polarization (DNP), now commonly called dissolution DNP. The latter is currently the most versatile and established method, and we herein propose to review the field of dissolution DNP from physical and biological perspectives (a comparison of the three techniques can be found in ref 10). The dissolution DNP technique has recently reached a point at which it is ready to move from proof-of-principle studies toward applications aimed at solving specific biological and medical problems. This shift has already started with an increasing number of articles published in biology-oriented and medical journals in the past few years. The motivation for this review at the current stage of evolution of the technique is to help (bio)medical researchers

Received: September 28, 2014

Revised: October 31, 2014

Published: November 4, 2014

understand the technology and determine if HP experiments can address questions in their own areas of interest.

## ■ PHYSICAL CONCEPTS AND TECHNICAL ASPECTS

The idea that electron spins can be used to enhance the polarization of nuclear spins was proposed in a seminal theoretical work by Overhauser<sup>11</sup> and was shortly thereafter confirmed experimentally by Carver and Slichter.<sup>12</sup> DNP found application in the field of particle physics for the production of polarized targets for scattering experiments<sup>13</sup> and also in solid-state nuclear magnetic resonance (NMR) where a host of researchers applied it to structural elucidation and analytical analysis in conjunction with magic-angle spinning (MAS) techniques, a method sometimes termed MAS DNP.<sup>14</sup> The feasibility of using DNP to directly enhance the water proton NMR signal in biological samples has also been demonstrated and even used *in vivo*,<sup>15</sup> and it is now commonly termed Overhauser DNP. However, the potential of DNP for investigating metabolism became clear only after the demonstration by Ardenkjaer-Larsen et al. that a frozen pellet of metabolically active compound could be dissolved while maintaining the large nuclear spin polarization that can be achieved at low temperatures.<sup>16</sup> To understand the value of this technique for *in vitro* and *in vivo* biological <sup>13</sup>C MRS studies, and the important parameters to take into account in experimental design, we present here the main physical concepts and some practical considerations.

The principle of DNP is to enhance the nuclear spin polarization by driving highly polarized unpaired electron spins out of thermal equilibrium, thereby allowing cross-polarization between electron spins and their surrounding nuclear spins. An external magnetic field for polarizing the spins and a microwave source for saturating the electron spin resonance (ESR) are thus required for DNP. Unpaired electron spins can be introduced inside the sample either chemically by adding persistent radicals or through gamma or UV irradiation.<sup>17–21</sup>

It is feasible to enhance the MRS signal by performing DNP *in situ*, i.e., directly within the biological system under investigation, but restrictions on the working field and temperature are imposed by the sample environment. For instance, MAS DNP experiments are usually performed at ~100 K and at high magnetic fields for compatibility with standard MAS NMR methods. The constraints are even tighter when Overhauser DNP has to be performed in living cells, or even *in vivo*, because the process has to take place at physiological temperature and, for potential human applications, in a magnetic field strength imposed by the available MRI scanner. The other two main issues inherent to *in situ* DNP are, first, the necessity to incorporate high concentrations of unpaired electron spins within the biological system, which might affect its physiology, and, second, heating due to the large microwave power required to saturate the ESR. In the context of *in vitro* and *in vivo* biological studies, the clear advantage of an *ex situ* method, such as dissolution DNP, coupled to a substrate injection protocol is that the field strength as well as the temperature at which the DNP processes take place can be chosen in a manner completely independent of the parameters used for the MR measurements. It is thus possible to select optimal temperature and field values to obtain the greatest substrate polarization within a given amount of time. Note that schemes based on *ex situ* Overhauser DNP were also proposed for biological studies, but the <sup>13</sup>C polarization that can be obtained is 3–4 orders of magnitude lower than the <sup>13</sup>C

polarization reached by dissolution DNP.<sup>22–24</sup> Therefore, *ex situ* Overhauser DNP cannot be used for <sup>13</sup>C MRS metabolic studies.

The two essential parameters determining the efficiency of DNP are the electron spin polarization ( $P_e$ ) and the electron spin longitudinal relaxation time ( $T_{1,e}$ ). At first approximation, the nuclear spin longitudinal relaxation time ( $T_{1,n}$ ) is not an independent parameter because it is directly proportional to  $T_{1,e}$  as the main relaxation mechanism of the nuclear spins is dipolar coupling to the unpaired electron spins. Ideally,  $P_e$  should be as large as possible and  $T_{1,e}$  sufficiently long to allow a saturation of the ESR with a minimal amount of power, thereby avoiding excessive sample heating. When these two parameters are evaluated as a function of temperature at 5 T (Figure 1), it is clear that the conditions are much more

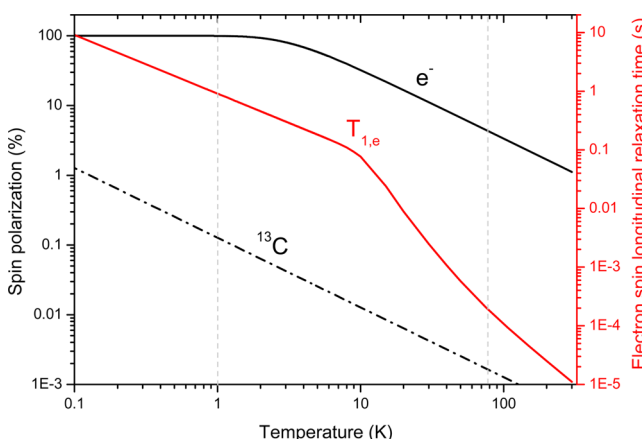


**Figure 1.** <sup>13</sup>C (dashed black curve) and electron (solid black curve) spin polarization at 5 T together with the electron spin longitudinal relaxation time (red curve) at 0.35 T as a function of temperature. The relaxation times for nitroxyl radicals were calculated from the fitting curved given in ref 25.

advantageous at 1 K than at liquid nitrogen temperature (77 K) or 300 K. Indeed, whereas at 1 K  $P_e$  is essentially 100% and  $T_{1,e}$  is close to 1 s, at 77 K the former is only ~4% and the latter is on the order of a few hundred microseconds, meaning that a much larger amount of power is required to saturate the ESR. The situation is clearly even worse at 300 K. Note that the values of  $T_{1,e}$  given here are only representative of nitroxyl radicals at 0.35 T,<sup>25</sup> but the temperature dependence of  $T_{1,e}$  for other radicals and at higher field strengths is expected to follow a similar trend.<sup>26</sup> Around 1 K, the maximal <sup>13</sup>C polarization that can be obtained via DNP is expected to be inversely proportional to the temperature, at least for samples containing wide-ESR-line-width radicals.<sup>17</sup> Whereas cooling and maintaining a sample at ~1 K via immersion in a bath of liquid <sup>4</sup>He at a pressure of ~0.1 mbar is rather straightforward, decreasing the bath temperature substantially below 1 K becomes technically much more challenging and requires the use of the rare and expensive <sup>3</sup>He isotope. Note also that at 1 K the <sup>13</sup>C polarization is only ~0.1% (Figure 1), which demonstrates that directly polarizing <sup>13</sup>C-labeled substrates without DNP (the brute force method) requires much more complex cryogenic technologies.

Besides the temperature, the other external parameter that can be adjusted to optimize the DNP process is the magnetic field. The original dissolution DNP apparatus was set to operate at 3.35 T,<sup>16</sup> but it has been shown that larger maximal

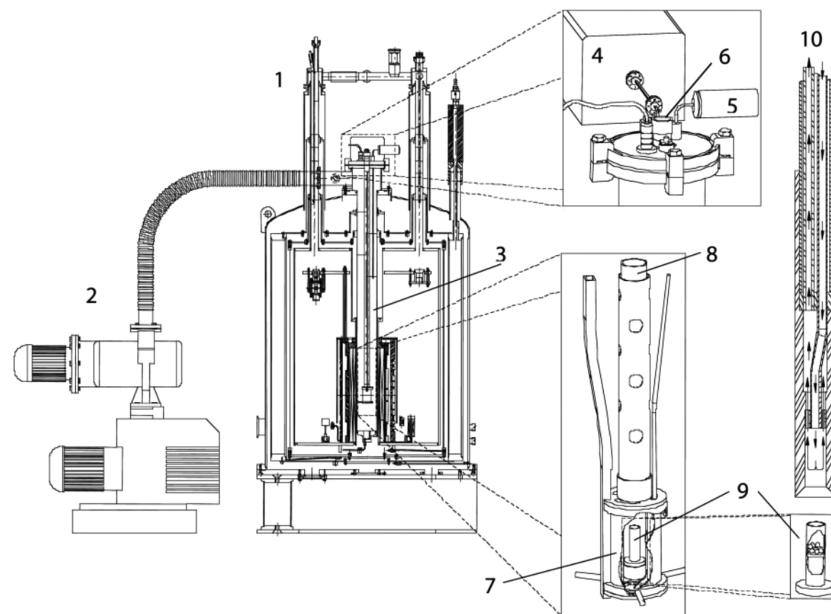


**Figure 2.** Schematic drawing of the original hyperpolarizer developed by Ardenkaer-Larsen et al.: (1) DNP polarizer, (2) vacuum pump, (3) variable-temperature insert, (4) microwave source, (5) pressure transducer, (6) sample port, (7) microwave container, (8) sample holder, (9) sample container, and (10) dissolution wand. Reproduced with permission from ref 16. Copyright 2003 National Academy of Sciences.

$^{13}\text{C}$  polarization can be obtained in a field of 4.6–5 T with all common radical types<sup>27,28</sup> and, at least with nitroxyl radicals, the maximal  $^{13}\text{C}$  polarization is even larger at 7 T.<sup>29</sup> A challenging technical issue arising when the field is increased is the fact that microwave losses become dramatically larger inside the transmission lines carrying the high-frequency microwaves from the source to the sample. Gold-plated or corrugated waveguides can be used to reduce these losses.<sup>29,30</sup>

On the basis of the information described above, it must be concluded that the higher the field and the lower the temperature, the larger the polarization. The drawback of working at a larger field and a lower temperature is that the polarization buildup times may become prohibitively long. A working temperature of 1 K and a magnetic field of 5 T thus seem to be a good compromise for dissolution DNP. Increasing the microwave power should aid in the acceleration of the polarization processes, but an exceedingly large power will lead to sample heating that will affect the polarization efficiency (the typical optimal power as measured at the microwave source output is on the order of 10–50 mW). A recent study showed that the maximal polarization expected when the ESR is fully saturated might be restricted due to sample heating.<sup>31</sup>

**Required Hardware.** The hyperpolarizer or dissolution DNP polarizer that needs to be coupled to a NMR or MRI instrument to perform HP MR consists of three main hardware components: (1) a superconducting magnet to set the external magnetic field, (2) a helium cryostat connected to vacuum pumps to cool the sample to ~1 K, and (3) a microwave source to enable the polarization transfer from the incorporated unpaired electron spins to the nuclear spins. The original system developed by Amersham Health based on a variable-temperature insert (Figure 2) has served as a basis for the implementation of the commercial HyperSense developed by Oxford Instruments. The HyperSense operates at 3.35 T and 1.2–1.6 K. A hyperpolarizer for clinical use (SPINlab) has been developed by GE Healthcare. It operates at 5 T and 1.1 K.

Alternative home-built systems have been implemented using room-temperature bore magnets.<sup>17,32–34</sup>

When installing a HP MR setup for metabolic studies, one must take into account the following practical considerations. (a) A helium recovery system is strongly recommended because the currently available preclinical systems require a substantial amount of liquid helium for running HP  $^{13}\text{C}$  MR experiments; SPINlab does however not require a supply of cryogenic liquids. (b) The quantification of the solid-state  $^{13}\text{C}$  polarization inside the hyperpolarizer is nontrivial because of the extremely long  $T_1$  and the short  $T_2$  inherent to  $^{13}\text{C}$  nuclear spins in frozen glassy samples at ~1 K. The authors suggest using a dedicated NMR spectrometer adapted for solid-state NMR measurements independent of the main MR system used for the biological studies. (c) An inadequate magnetic field profile between the hyperpolarizer and the main NMR/MRI magnet can lead to a dramatic reduction in the liquid-state  $^{13}\text{C}$  polarization of the substrate (this will be further discussed in the following sections). The location of the hyperpolarizer with respect to the MR system is thus crucial and should be carefully chosen. Once the hardware and the physical parameters of the sample environment have been optimized, the sample chemical composition needs to be carefully adjusted to maximize the  $^{13}\text{C}$  polarization of metabolic substrates.

**Impact of the Choice of Radical.** In a field of 3–7 T and at a temperature of ~1 K,  $^{13}\text{C}$  polarizations on the order of 10–50% can be typically reached within a few hours. The maximal nuclear polarization and the time necessary to reach it strongly depend on sample content and preparation. Radicals, also called polarizing agents, and solvents are the crucial components that must be carefully selected. The typical concentration of polarizing agents is in the range 15–60 mM, and to date, trityl radicals and the persistent 1,3-bis(diphenylene-2-phenylallyl) (BDPA) radical have proven to be the most efficient agents for polarizing  $^{13}\text{C}$ -labeled substrates.<sup>16,35</sup> One of the most important characteristics of a radical in the context of DNP is its ESR line width, which correlates with the width of the

frequency-dependent  $^{13}\text{C}$  polarization enhancement microwave spectrum (Figure 3). The essential feature behind the high

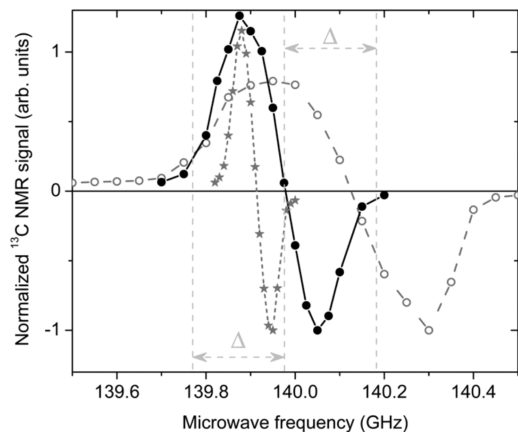


**Figure 3.** Microwave spectra at 5 T and 4.2 K. Comparison between the microwave spectra measured by  $^{13}\text{C}$  MR in  $[1\text{-}^{13}\text{C}]$ pyruvic acid doped with 16 mM OX063 trityl radicals (\*), UV-irradiated  $[1\text{-}^{13}\text{C}]$ pyruvic acid (●), and a frozen 3 M sodium  $[1\text{-}^{13}\text{C}]$ pyruvate aqueous solution doped with 50 mM TEMPO nitroxyl radicals (○). The frequency separation  $\Delta$  between the central and the left or right vertical dotted lines corresponds to the  $^1\text{H}$  MR frequency at 5 T. Reproduced with permission from ref 19. Copyright 2013 National Academy of Sciences.

DNP efficiency of radicals such as trityls is that their ESR line width is narrower than the  $^1\text{H}$  resonance frequency. As a consequence, the probability of enabling electron spins to cross-polarize proton spins using microwave irradiation is very low, increasing the probability of polarization transfer to  $^{13}\text{C}$  spins and thereby producing larger maximal  $^{13}\text{C}$  polarization. It has however been observed that the  $^1\text{H}$  polarization reaches a level nearly 4 times higher than the  $^{13}\text{C}$  polarization in typical nitroxyl-doped samples used in dissolution DNP, and that the characteristic polarization buildup time constant is substantially shorter for  $^1\text{H}$  than for  $^{13}\text{C}$ .<sup>36</sup> Researchers can take advantage of the fact that nitroxyl radicals efficiently and rapidly polarize protons to obtain large  $^{13}\text{C}$  polarizations in a short amount of time through  $^1\text{H}$ - $^{13}\text{C}$  cross-polarization schemes, although the maximal  $^{13}\text{C}$  polarization in the liquid state is still lower than the levels obtained using BDPA or trityl radicals.<sup>37</sup> Solvent deuteration leads to increased maximal  $^{13}\text{C}$  polarization with wide-ESR-line-width polarizing agents such as nitroxyl radicals, whereas it causes a reduction in maximal  $^{13}\text{C}$  polarization when trityl or BDPA is used.<sup>36,38</sup> It must be stressed that although the maximal  $^{13}\text{C}$  polarization that can be reached in samples doped with the widely available nitroxyl radicals will generally not be as large as in trityl- or BDPA-doped samples, the difference will not exceed a factor 2–3 for most substrates in optimized sample preparations, which makes nitroxyl radicals suitable for *in vitro* and *in vivo* preclinical studies (see, e.g., ref 39). The nonpersistent radicals that can be photoinduced in frozen pyruvic acid following UV irradiation at liquid nitrogen temperature do not exhibit an ESR line width as narrow as that of trityls or BDPA, but it seems to be narrow enough to limit proton polarization (Figure 3), with the additional advantage of not requiring a filtration process prior to injection into subjects.<sup>19,40</sup>

It was demonstrated that the maximal  $^{13}\text{C}$  polarization that can be achieved at 3.35 T and 1.2–1.4 K can be more than

doubled by adding  $\text{Gd}^{3+}$  compounds or complexes to the sample,<sup>41</sup> but this considerable improvement seems to be restricted to samples prepared with trityl radicals.<sup>42</sup> The incorporation of  $\text{Gd}^{3+}$  in trityl-doped samples also accelerates the  $^{13}\text{C}$  polarization buildup, and it is now widely used in the composition of many substrate preparations for dissolution DNP.<sup>43</sup>

In the following two sections, we describe the crucial steps to minimize the  $^{13}\text{C}$  polarization losses during the process of bringing the DNP-enhanced  $^{13}\text{C}$ -labeled metabolic substrates from the polarizer 1 K environment into the biological system under MR investigation.

**From Solid to Liquid: The Key Dissolution Step.** As already mentioned above, the groundbreaking innovation that brought DNP into the realm of *in vitro* and *in vivo* biological MR was the addition of a dissolution procedure for producing HP liquid-state imaging agents at physiological temperatures.<sup>16</sup> Dissolution is performed by propelling a hot solvent onto the frozen sample to rapidly melt it. The resulting solution is chased out of the polarizer using pressurized helium gas and collected for injection into an NMR tube, an animal, or a human. The technique has been used to hyperpolarize  $^1\text{H}$ ,  $^6\text{Li}$ ,  $^{13}\text{C}$ ,  $^{15}\text{N}$ ,  $^{89}\text{Y}$ , and both  $^{107}\text{Ag}$  and  $^{109}\text{Ag}$ ,<sup>16,44–51</sup> and the liquid-state nuclear polarizations are typically enhanced by 3–4 orders of magnitude compared to the room-temperature thermal polarizations at common magnetic field strengths. A pivotal point that has made dissolution DNP feasible was the determination of the appropriate environment in which to perform the solid-to-liquid phase transformation. It is indeed required to nearly instantaneously cross the region of the magnetic field-temperature parameter space where  $4.2 \text{ K} < T < T_{\text{melt}}$  in which  $T_{1,n}$  can become extremely short, especially at low magnetic field, because of the presence of the paramagnetic centers embedded inside the DNP-enhanced frozen sample ( $T_{\text{melt}}$  is defined as the melting temperature of the sample). The key for the dissolution step is thus to use a hot solvent with a large heat capacity to rapidly melt the frozen sample (water has the highest specific heat capacity of all solvents that are liquid at room temperature) and to perform the dissolution *in situ*, in the low-temperature and high-magnetic field environment set for DNP, i.e., inside the cryostat placed in the bore of the superconducting magnet. When persistent radicals are used for the solid-state DNP process, their dilution in the solvent also reduces the paramagnetic spin relaxation rate.

**Transfer and Injection of Hyperpolarized  $^{13}\text{C}$  Substrates.** The DNP-enhanced  $^{13}\text{C}$ -labeled substrates, once dissolved in hot water, have to be rapidly transferred into the bore of the MR system to minimize the  $^{13}\text{C}$  polarization losses occurring through longitudinal spin relaxation processes (the standard room-temperature  $T_1$  of  $^{13}\text{C}$ -labeled metabolic substrates is shorter than 1 min<sup>43</sup>). The  $^{13}\text{C}$  spins will usually experience drastic magnetic field variations during the transfer, and for many substrates,  $T_{1,n}$  becomes extremely short in the low-field region located between the two magnets. For this reason, the distance between the hyperpolarizer and the MR instrument should be kept as short as possible and a fast transfer procedure is greatly important.  $T_{1,n}$  is influenced by the chemical environment of the nuclear spins, the magnetic field, and the temperature. Field and temperature are in most cases imposed by the experimental conditions and can often not be set to optimal values. Note that when the solution containing the HP  $^{13}\text{C}$ -labeled substrates is being transferred, it is mandatory not to cross very large gradients (avoid, for instance,

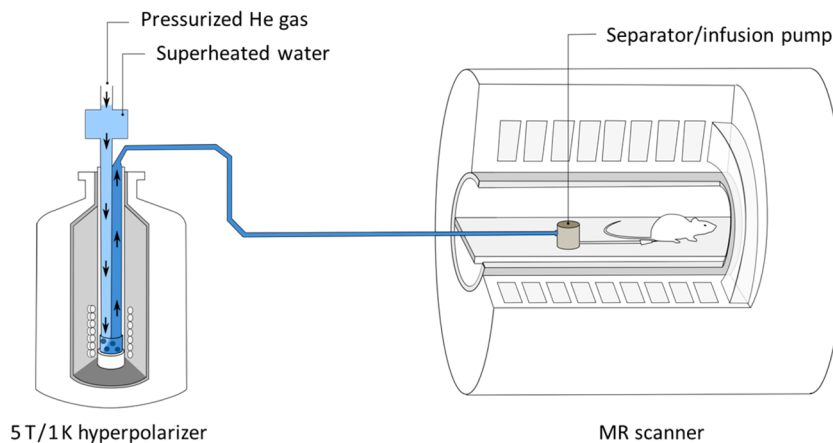


**Figure 4.** Sketch of the dissolution DNP setup installed at the Center for Biomedical Imaging (CIBM) of the Ecole Polytechnique Fédérale de Lausanne (EPFL). A 5 T, 1 K hyperpolarizer is located ~4 m from a 9.4 T rodent MR scanner. A specific device minimizing the delay between the dissolution and the infusion of DNP-enhanced molecules has been implemented for *in vivo* applications. The delay can be as short as 3 s.<sup>52</sup>

passing the solution in the proximity of strongly magnetized material) to avoid destroying the  $^{13}\text{C}$  polarization via nonadiabatic passage; the reviewers also advise to map the field between the hyperpolarizer and the MR system to determine where the low-field regions are located and whether the solutions containing the HP substrates should be transported within a permanent magnet. In terms of temperature, the solution can be rapidly thermalized using an appropriately controlled container, thus allowing the establishment of an optimal temperature for minimizing the relaxation prior to injection (Figure 4).<sup>52</sup> The chemical environment of the nuclear spins can be partially controlled by choosing an appropriate solvent (deuteration helps reduce the nuclear dipolar relaxation) and by reducing the concentration of paramagnetic centers dissolved in the HP solutions.<sup>35,52,53</sup> Isotopic substitution can also be used to reduce the intramolecular relaxation in the molecules of interest. In many cases, the main relaxation mechanism is via interactions with paramagnetic impurities. Because paramagnetic centers are required for the DNP process, the solution usually contains a substantial amount of radicals, unless nonpersistent radicals are used like in the method proposed by Eichhorn et al.<sup>19</sup> These radicals need to be filtered, using an anion-exchange or reverse phase column or polyethylene filters,<sup>16,35,54,55</sup> or scavenged with an antioxidant such as vitamin C.<sup>52,53</sup> Note that it has been shown that on specific molecules it is possible to store the enhanced polarization in long-lived singlet states, the relaxation times of which can be >10 times longer than the  $T_1$  of the nuclear spins forming the singlet states.<sup>56,57</sup>

**Optimizing  $^{13}\text{C}$  MR Acquisition.** Following the injection of the HP  $^{13}\text{C}$ -labeled substrates, the nuclear polarization will inevitably and irreversibly decrease back to its thermal equilibrium value, and the typical time window available for performing a metabolic study is on the order of 1 min. The polarization decay will additionally be accelerated by the application of the radiofrequency pulses that are used to perform the MR measurements. How long the signal will be detectable will depend on the sensitivity (noise level) and the magnetization flip angle related to the radiofrequency pulses. Several schemes have been proposed to perform multiecho acquisitions or to use spatially and spectrally selective radiofrequency excitations to increase the time over which the HP nuclear spins can be measured by limiting the amount

of enhanced longitudinal magnetization that is required for each acquisition.<sup>58–61</sup> It is also possible to highly enhance and detect nuclear spins with short relaxation times via *in vitro* or *in vivo* polarization transfer from long- $T_1$  HP nuclear spins.<sup>50,62,63</sup> Such methods can potentially lead to increased sensitivity or increased spectral resolution even *in vivo*.<sup>64</sup> A complete review of the acquisition schemes and hardware is beyond the scope of this review, and it is the reviewers' opinion that, to date, no all-purpose or standard scheme has been defined. Each type of MR experiment will most likely require its own optimal scheme because of the irreversible destruction of the  $^{13}\text{C}$  magnetization after each acquisition.

## BIOLOGICAL APPLICATIONS

As one can gather from the introduction to hyperpolarization technology, the chemistry and physics of DNP is a field unto itself. While the current versions of commercially available hyperpolarizers are designed for turnkey operation, the researcher would do well to understand some of the finer points of the process to avoid misinterpretation of data. Basic physical sciences are however not driving the development of this technology; it is the biomedical applications that have animated the field, as DNP-enhanced  $^{13}\text{C}$  MRI has unique potential as a molecular imaging tool. First, the technology does not use ionizing radiation, so its repeated use in children or in other vulnerable populations is not restricted in any way. Second, with the chemical shift that is endemic to the MR technique itself, kinetics of chemical reactions are naturally detected, not simple uptake of a substrate. The specificity of MR-based methods is rivaled only by mass spectrometry, which is limited to *ex vivo* samples. To aid the reader in gaining a global understanding of the power of the method as well as its weaknesses, the review of the biological applications is broken down into pathways as opposed to a review of current agents. For a very complete review of available agents, see ref 65. A particularly helpful overview of the targets and/or challenges of imaging cancer with HP agents was published recently as well.<sup>66</sup> Krishna et al. have also published an insightful review that surveys methods for measuring tissue oxygen partial pressure ( $\text{pO}_2$ ) as well as intermediary metabolism using HP methods,<sup>67</sup> a work similar in scope to the review published by Tyler in 2011.<sup>68</sup>

## ■ GLYCOLYSIS

Glucose metabolism is subject to control at multiple points within the glycolytic pathway.<sup>69</sup> Warburg proposed nearly 70 years ago that glycolysis and lactic acid fermentation was the primary cause of cancer.<sup>70</sup> While this theory has been disproven, abundant lactate is nonetheless phenotypically conserved across most cancer cell types. Much like the detection of cancer drove the early development of MRI itself, cancer diagnosis is the most obvious “killer application” for imaging with probes that reflect glycolytic metabolism.<sup>71</sup> HP glucose itself is the most obvious agent for detecting glycolytic flux, but the short  $T_1$  of the protonated carbons can limit its effective use. [U- $^{13}\text{C}_6\text{U}^2\text{H}_7$ ]Glucose has therefore been the primary metabolite used in studies to date, as the deuteration removes the effects of  $^1\text{H}$ - $^{13}\text{C}$  dipolar relaxation, increasing the  $T_1$  to  $\sim 10$  s for each site. The first application of this probe was in yeast, where *Saccharomyces cerevisiae* rapidly metabolized the glucose to a variety of downstream metabolites.<sup>72</sup> Experiments in cell culture were completed using a high-resolution NMR system, where line shape and the small coil volume allowed optimal shimming conditions and rapid detection of metabolism (Figure 5). Every metabolite in the glycolytic chain was

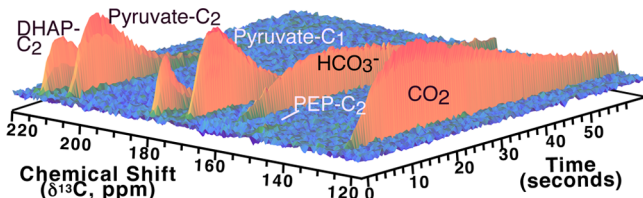


**Figure 5.** Aliphatic region of the  $^{13}\text{C}$  NMR spectrum acquired after injection of HP [ $\text{U}^2\text{H},\text{U}^{13}\text{C}$ ]glucose into yeast cell culture shown as a surface plot with time on the y-axes. Stepwise kinetics of each enzyme in glycolysis was observed.

detected, each showing a delay in the kinetics that was appropriate for its position in the pathway relative to the glucose probe. The visually striking data demonstrate the power of DNP-NMR for detecting kinetics in living systems.

Frydman and co-workers used the same probe in T47D breast cancer cells and noted a similar set of metabolites.<sup>73</sup> Using a shaped pulse detection scheme, they were also able to make estimates of kinetics for enzyme-catalyzed reactions that do not require direct detection of the intermediate species. The power of this technique has not been fully grasped by the HP imaging community at large, and methods like this deserve extended development in the opinion of the reviewers. Unfortunately, normal mammalian tissues do not have glycolytic rates that are as high as those of yeast or cancer cells, as *in vivo* mouse studies have initially failed to detect the metabolism of glucose.<sup>74</sup> This somewhat disappointing result was confirmed in the work of Rodrigues et al. in which heart, brain, and kidney all failed to produce HP lactate subsequent to the injection of the HP glucose probe.<sup>75</sup> However, the work of Rodrigues was focused on detecting cancer, and in orthotopically implanted EL4 and LL2 tumor lines, metabolism of glucose to lactate was detected and imaged in real time (Figure 6). It should be mentioned that the method used is analogous to 2-deoxy-2-[ $^{18}\text{F}$ ]fluorogluucose (FDG) positron emission tomography (PET), with the exception that the actual metabolic flux is detected as opposed to simple probe uptake. FDG-PET retains a large absolute sensitivity advantage, but the

DNP method might be superior when it is imperative to measure *in vivo* enzyme kinetics. Very recently, HP [U- $^{13}\text{C}_6\text{U}^2\text{H}$ ]glucose has been used to measure cytosolic NAD $^+$ /NADH ratios in cancer cell culture.<sup>76</sup> Strong correlations were found between the lactate/pyruvate ratio as detected by HP-NMR and the cytosolic redox state.

Glycolytic metabolism is of course active in the heart, liver, muscle, brain, etc., but the failure to detect its metabolism (to date) using HP glucose illustrates that a variety of factors influence the sensitivity of the experiment. The detected signal intensity is a product of several factors:

$$\text{signal} = \% \text{ polarization} \times \text{pool size} \times \text{fractional enrichment} \quad (1)$$

This value is of course convolved with the sensitivity of the MR hardware. Even though these tissues can turn over large amounts of glucose daily, the kinetics on the time scale of  $\sim 1$  min has been slow enough to prevent detection so far. Glucose has not been polarized as effectively as pyruvate or other targets to date, for reasons that are not easily explained. A typical value is  $\sim 20\%$ , while pyruvic acid with the trityl radical can easily yield twice that number. Given the data presented so far, significant advances in the production and delivery of HP glucose will be needed to detect flux in any case outside of cancer metabolism. Physiologic states (besides cancer) that emphasize glucose utilization, i.e., brain metabolism or heart failure, may be the targets most likely to produce significant results.

Another tack on measuring glycolytic flux is simply determining the size of the lactate pool in the targeted tissue. Detection of lactate in tissue by  $^1\text{H}$  MR spectroscopic imaging methods is difficult because of its low concentration [low signal-to-noise ratio (SNR)] and because it co-resonates with the methylene protons of fat. Imaging the lactate concentration with HP pyruvate does not suffer from any background signals because of the unique  $^{13}\text{C}$  chemical shift of all the carbons of lactate. In practice, a number of considerations have made pyruvate the imaging agent of choice not just for cancer detection but for a variety of experiments in living systems. Pyruvic acid makes an ideal target for DNP in the solid state. Neat pyruvic acid will solubilize the trityl radical, allowing high concentrations of the  $^{13}\text{C}$  isotope to be attained. Higher concentrations of isotope speed the polarization process.<sup>17</sup> The neat acid also has few protons, which can increase the absolute polarization levels.<sup>38</sup> Following dissolution, the NMR properties of pyruvate are favorable, as well. The C1 and C2 positions of pyruvate are not protonated and hence have long  $T_1$  values ( $\sim 1$  min) at 3 T, which preserves the HP magnetization for periods long enough to image using even relatively slow protocols like chemical shift imaging (CSI). Pyruvate exchange with lactate is catalyzed by lactate dehydrogenase, an enzyme common to every tissue type. The production of lactate from pyruvate consumes a reducing equivalent derived from NADH, and the reverse reaction transfers a hydride to NAD $^+$ . The NAD $^+$ /NADH ratio maintained under normal physiological conditions manifests as a 10/1 lactate/pyruvate ratio in the cytosol.<sup>77</sup> In cells exhibiting high levels of anaerobic (as in exercising muscle) or aerobic (as in the Warburg effect) glycolysis, the lactate level can increase significantly. HP [1- $^{13}\text{C}$ ]pyruvate was first used to image cancer by the original developers of the dissolution technique in a rat model.<sup>78</sup> Using a simple CSI protocol, an enhanced lactate signal was detected in a P22 tumor model. These first images exerted a tremendous

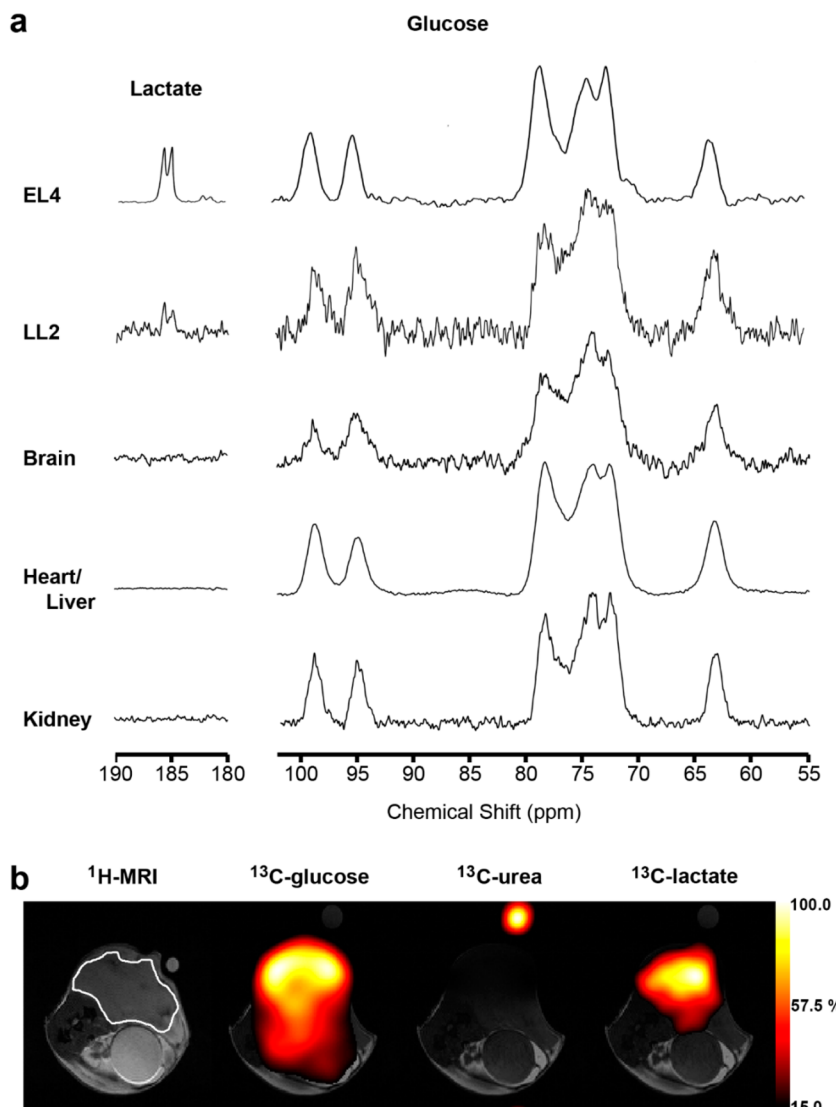


**Figure 6.** (a) Glycolytic metabolism in subcutaneously implanted xenografts of EL4 and LL2 cancer cell lines as detected with HP [<sup>2</sup>H,<sup>13</sup>C]glucose. Note the lack of lactate signal detected in normal tissues. (b) Images of glycolytic metabolism in the EL4 cancer model. Courtesy of Kevin Brindle.

influence on the field, as the diagnostic potential of the technique was apparent. The authors proposed that ratiometric imaging, images based on the ratio of a metabolite to the parent pyruvate signal, might carry the most diagnostic potential. It is important to understand that any ratio of intensities observed probably does not represent the actual concentrations of the metabolites because of the confluence of eq 1 and the vascular concentrations of the probe that is delivered. For this reason, comparison of ratios of upstream versus downstream metabolites between control and experimental groups is a ubiquitous method for extracting metabolic information from HP experiments. Almost immediately, a flurry of papers reported on various aspects of pyruvate metabolism in tumor tissue. Day et al. were the first to use HP pyruvate to detect the response to the treatment of a cancer cell line.<sup>79</sup> Treatment of EL-4 cancer cells with etoposide resulted in lower apparent rate constants for pyruvate to lactate flux,  $k_{PL}$ , while the activity of lactate dehydrogenase (LDH) was not significantly changed. Interestingly, the impact of pool size (eq 1) on the HP signal intensity was first investigated in this paper, where the addition

of exogenous lactate to the cell culture allowed serially increasing HP [<sup>1</sup><sup>3</sup>C]lactate signals to be observed. A discussion of modeling of the kinetics of the HP species is presented in a following dedicated section.

*In vivo* experiments at the University of California San Francisco (UCSF) using a transgenic adenocarcinoma model of a mouse prostate (TRAMP) mouse illustrated a new method for acquiring chemically selective images.<sup>80</sup> While a review of imaging sequences is not our goal, the echo planar spectroscopic imaging (EPSI) sequence<sup>81</sup> used represented a significant acceleration in the speed of acquisition of dynamic data in living animals, reducing the time needed for consecutive images to 3 s. Lactate resonances were detected in the liver, muscle, and kidney, but the tumor region produced the highest lactate/pyruvate ratio as expected. The same team quickly followed this work with a study designed not only to detect but also to grade tumors using the same TRAMP model.<sup>82</sup> From a development perspective, this paper was the first to build a metric based on the total HP carbon (THC) for analysis of the results. THC integrates the total intensity for every resonance

as a function of time to produce a total signal for normalization of each individual resonance. In this way, the method works much like total activity measurements in radioactive tracer experiments. A plot of the THC versus the HP lactate SNR showed an increasing THC value in the tumor as a function of tumor grade, as well as grade-dependent increases in the lactate signal. Higher THC values in the tumor were rationalized by increased levels of expression of monocarboxylate transporters (MCTs) in the higher-grade tumors. Park et al. applied HP pyruvate imaging to an orthotopic brain tumor model, generating a large number of significant differences between control and experimental groups.<sup>83</sup>

Subsequent studies by the UCSF team have probed the effects of phosphatidylinositol 3-kinase inhibition<sup>84</sup> and hypoxia-inducible factor-1 and Myc activity on the production of HP lactate.<sup>85</sup> Both these papers were encouraging for the field, as they applied <sup>13</sup>C imaging *in vivo* in a straightforward, reproducible manner to gain insight into metabolic questions without emphasizing technology development; publications of this nature emphasize a “coming of age” of the technology. Similar observations relating tumor viability to the lactate/pyruvate ratio were made by Senadheera et al.<sup>86</sup> They observed that radiation treatments decreased the lactate/pyruvate ratio significantly in tumors from the TRAMP model. Other work by Seth et al. hypothesized that reduced flux through LDH would result in negative consequences for tumor viability, and that treatment of tumors with dichloroacetic acid (DCA) would enhance the vulnerability of tumors to further treatment.<sup>87</sup> DCA enhances oxidation of pyruvate, effectively draining the pool of pyruvate that would naturally exchange with lactate. Indeed, DCA treatment not only lowered the lactate/pyruvate ratio but also enhanced the sensitivity of tumors to therapeutic paclitaxel doses. Experimentally, this paper highlights the unique kinetic information that can be collected using HP methods, but it also illustrates just how complicated modeling of the phenomena can be. A decreased lactate signal can arise from increased exchange or flux of pyruvate into other pools of metabolites, not just a change in the activity of the enzyme catalyzing the reaction of interest. In a similar vein, the hypothesis that interrupted glycolytic metabolism could further sensitize tumors to radiation treatment was tested using HP pyruvate in an anaplastic thyroid cancer (ATC) model.<sup>88</sup> Sandulache et al. demonstrated that 2-deoxyglucose (2-DG) significantly inhibited the generation of HP [<sup>1-13</sup>C]lactate production in xenografts of established ATC cell lines. Using a variety of assays of cell viability, the authors confirmed that inhibition of glycolytic flux increased the efficacy of radiation treatment but ultimately concluded that drugs more effective than 2-DG would be necessary to show similar effects in human cancers. Recently, the same group has studied the generation of reactive oxygen species (ROS) by radiation treatment of the same ATC model.<sup>89</sup> The impact of ROS on the reductive potential of cancer cells changed the availability of NADH in the cytosol, thereby downregulating HP [<sup>1-13</sup>C]lactate production. Further insight into the phenomena governing the amplitude of the lactate signal was gained by Bohndiek and co-workers; they used a battery of examinations to study the effects of bevacizumab on tumor progression in a mouse model of colorectal cancer.<sup>90</sup> This study used dynamic contrast enhanced (DCE) and diffusion-weighted MRI to measure tumor perfusion and necrosis. In addition to [<sup>1-13</sup>C]pyruvate, the HP protocol included [1,4-<sup>13</sup>C<sub>2</sub>]fumarate, which is a marker of tumor necrosis.<sup>91</sup> These experiments showed that a

weakened lactate response originated from reduced tumor perfusion (reduced delivery of the HP pyruvate precursor), not necessarily from a change in the kinetics of LDH. LDH inhibition can, however, certainly control the appearance of lactate, as well, as evidenced in a lymphoma model.<sup>92</sup> In contrast, the lab of Ronen compared the MCF-7 breast cancer cells to PC3 prostate cancer cells under treatment with a mitogen-activated protein kinase inhibitor.<sup>93</sup> The MCF-7 cells showed a similar decrease in the level of lactate generation upon treatment, but the prostate cancer cell line showed an increased level of lactate generation. Assays of the cellular redox state, LDH expression and activity, and intracellular lactate levels yielded similar increases across both cell lines. Ultimately, downregulation of MCT expression was used to rationalize the difference in HP lactate levels, but the complexity of the system reiterates the necessity of a global view of intermediary metabolism and enzyme expression and/or activity for interpretation of the HP pyruvate results. In one of the few papers to discuss a negative result, Butt et al. did not note significant changes in pyruvate to lactate flux when tamoxifen was used to treat a breast cancer model.<sup>94</sup> It should be noted that only the apparent rate constant was measured; analysis of areas under the curve was omitted for unknown reasons. Most recently, the connection between tumor lactate and higher metastatic potential has been probed in another model of breast cancer.<sup>95</sup> In a somewhat surprising observation, metastatic risk was positively correlated with a decreased pyruvate to lactate rate constant. Once again, the surprising differences in the apparent rate constant were rationalized by changes in the lactate pool size. Somewhat related to these applications to cancer metabolism is the recent examination of the effects of radiation upon the observed lactate/pyruvate ratio in radiation-damaged rat lung.<sup>96</sup> An increase in the lactate/pyruvate ratio was attributed to the onset of inflammation associated with the radiation damage. Strong positive correlations between the lactate/pyruvate ratio and the macrophage count produced a convincing narrative about the effectiveness of HP pyruvate for the detection of inflammation.<sup>97</sup>

FDG-PET is a clinically well-established technique that assays glucose uptake that presages glycolytic flux. It is quite natural that comparisons be made between FDG-PET and HP pyruvate imaging. Witney et al. were the first to compare the two methods using the lymphoma model common to their experiments and an etoposide treatment regimen.<sup>98</sup> Treatment of the tumor produced changes in FDG uptake within a short time span, but the conversion of HP pyruvate to lactate was downregulated only after a longer treatment regimen. Ultimately, the authors suggested that HP pyruvate might be a superior imaging agent when used in the brain to detect tumors (high level of background uptake) or prostate cancer (low level of glucose uptake). A more comprehensive comparison of resolution and other imaging parameters was not given. A similar study design was used by Weidl and co-workers in a model of hepatocellular carcinoma,<sup>99</sup> but a final comparison of the relative merits of the imaging modalities was not forthcoming. The authors suggested that a combination of FDG-PET and HP pyruvate imaging might be advantageous, as the information content of such an experiment would exceed the individual contributions.

## ■ OXIDATIVE FLUX

In addition to the aforementioned favorable properties of pyruvic acid as a substrate for the DNP process, pyruvate can

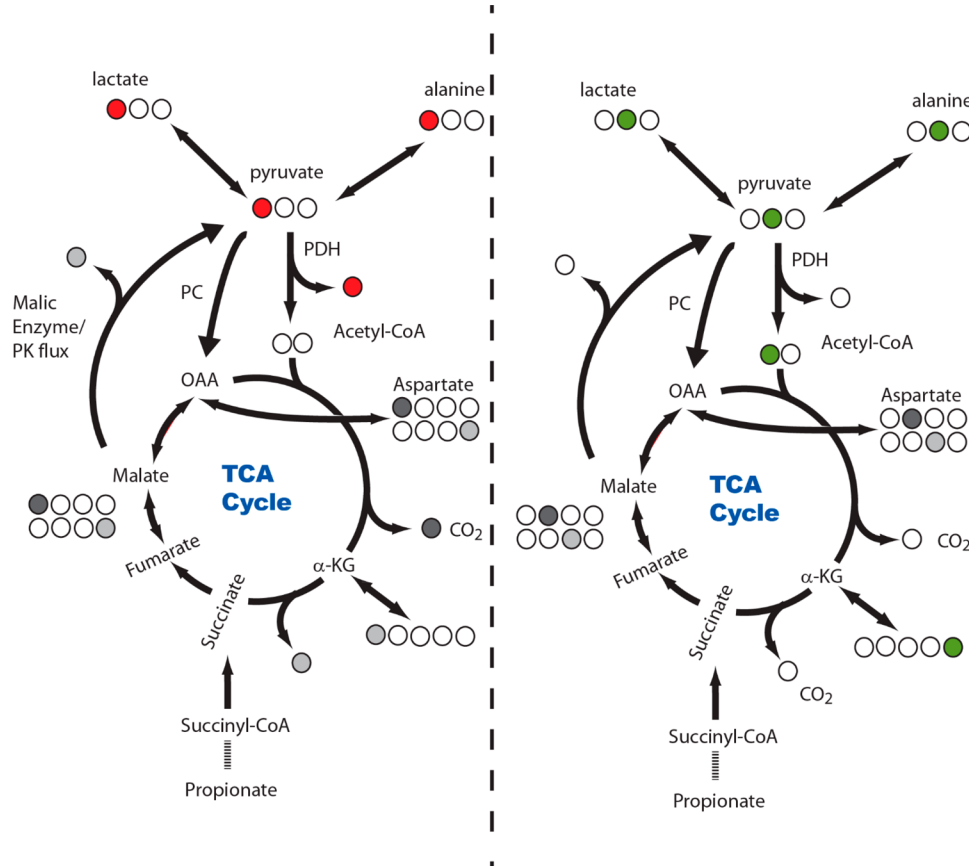


**Figure 7.** Distribution of the  $^{13}\text{C}$  label following metabolism of  $[1-^{13}\text{C}]$ - or  $[2-^{13}\text{C}]$ pyruvate. Four alternate pathways for producing HP  $[^{13}\text{C}]$ bicarbonate exist, including PDH flux, a forward turn of the TCA cycle after pyruvate carboxylation, or alternately flux through pyruvate kinase (PK) or the malic enzyme. PK acts to decarboxylate oxaloacetate as opposed to malate.

transit the pyruvate dehydrogenase complex, yielding a  $\text{CO}_2$  and an acetyl-CoA that can be subsequently oxidized in the tricarboxylic acid (TCA) cycle (Figure 7). Oxidative phosphorylation depends upon the reducing equivalents generated by the TCA cycle. The acetyl-CoA that condenses with oxaloacetate to make citrate at the entry point of the TCA cycle can be derived from carbohydrates, fatty acids, or ketones. Glycolysis directly produces pyruvate, and lactate can also be easily oxidized because of the abundance of lactate dehydrogenase in most tissues. Likewise, alanine amino transferase (ALT) allows alanine oxidation through pyruvate. However, alanine's primary fate is transport to the liver; its production usually presages the transport of nitrogen back to the liver for disposal as urea.<sup>100</sup> Of the three-carbon glycolytic products, pyruvate has dominated hyperpolarization in practice, despite compelling arguments that either lactate or alanine (each more abundant in living systems) should be a superior imaging substrate. It is clear that supraphysiologic concentrations of the agent are needed for HP imaging, even with the increased sensitivity provided by DNP. However, this is a case in which the short time window for the imaging experiment determined by the  $T_1$  of the agent is an advantage. The high concentrations injected do not produce large changes in metabolite pool sizes on the time scale of the experiment, at least in the perfused heart.<sup>101,102</sup> The data presented in these two studies has been underappreciated in the literature, to the detriment of the entire field of HP studies of metabolism. The essential conclusion of the papers is this: the bolus of HP material intended for use as an imaging agent does not affect intermediary metabolism

before the useful kinetic information has been measured. The HP experiment essentially produces a snapshot of normal metabolism at the time of injection. Further papers addressing dose-dependent aspects of kinetic measurements are important experimentally but do not address the direct biological consequences of a pyruvate bolus.<sup>103,104</sup> Furthermore, the multiplicity of metabolic fates for pyruvate makes it an ideal substrate for molecular imaging, as it can report on a host of enzyme-catalyzed reactions in living systems. Pyruvate and lactate both are translated into the cytosol via a monocarboxylate transporter (MCT1).<sup>105</sup> This is a kinetic advantage for the rapid delivery of the polarized molecule to the intracellular machinery. Alanine transport is primarily electrogenic in nature and has kinetic properties similar to those of lactate and pyruvate transport.<sup>106</sup> A factor that distinguishes pyruvate from other three-carbon intermediates is its low abundance relative to that of lactate and alanine. This means that a bolus of pyruvate can exchange into the larger lactate and alanine pools, producing intense resonances as measured as a fraction of the total carbon signal. Instances in which lactate or alanine is used as the imaging probe typically produce lower SNR for the downstream metabolites than for pyruvate.<sup>82,107</sup> Nonetheless, HP  $[1-^{13}\text{C}]$ lactate oxidation can be detected in skeletal muscle if experimental parameters are optimized.<sup>108</sup> Pyruvate itself was first used as an agent in the work of the original team led by Golman.<sup>109</sup> All the advantages of  $[1-^{13}\text{C}]$ pyruvate were used to good effect, as  $[1-^{13}\text{C}]$ lactate,  $[1-^{13}\text{C}]$ alanine, and  $[^{13}\text{C}]$ -bicarbonate were detected. The HP  $[^{13}\text{C}]$ bicarbonate generated from  $[1-^{13}\text{C}]$ pyruvate is a direct readout of flux through the

pyruvate dehydrogenase complex and is hence correlated with the production of acetyl-CoA from pyruvate (Figure 7). If the  $^{13}\text{C}$  label is placed at the C2 position of pyruvate, the label is passed to acetyl-CoA, where it can be subsequently detected in citrate or glutamate. Pyruvate dehydrogenase (PDH) flux in the heart is the primary and probably the only source of [ $^{13}\text{C}$ ]bicarbonate when HP [ $1\text{-}^{13}\text{C}$ ]pyruvate is used as the imaging agent.<sup>110</sup> Merritt and co-workers demonstrated that PDH flux, and therefore HP [ $^{13}\text{C}$ ]bicarbonate generation, could be modulated by the availability of a medium-chain fatty acid in the perfused heart. Furthermore, they suggested that the appearance of both bicarbonate and  $\text{CO}_2$  in the measurements might facilitate an estimate of pH in the tissue, a goal that became the subject of further publications by multiple groups.<sup>111,112</sup>

Similar observations about competition between fatty acid and pyruvate metabolism were made in the rat *in vivo*, where fasting was shown to decrease the rate of appearance of HP [ $^{13}\text{C}$ ]bicarbonate, presumably because of the increased availability of free fatty acids.<sup>113</sup> Induction of type 1 diabetes by streptozotocin treatment produced similar changes in PDH flux. *In vivo* spectra were acquired using a simple surface coil arrangement with no other source of localization. Almost concurrently, the progenitors of the dissolution DNP technique produced some of the most compelling images that have been observed in the heart using a porcine model of myocardial infarction and a relatively simple CSI method.<sup>114</sup> Brief local ischemia or alternately infarction was achieved using a balloon catheter for either 15 or 45 min to produce an occlusion in the left circumflex artery. Once the occlusion was released, subsequent images obtained with the injection of HP [ $1\text{-}^{13}\text{C}$ ]pyruvate showed the restoration of perfusion, as measured by the specific lactate or alanine measurements, but decreased PDH flux. Furthermore, the longer occlusion time produced images that showed a larger defect in [ $^{13}\text{C}$ ]bicarbonate production. Confirmation of reperfusion was validated using a standard gadolinium-based method. These observations animated the field of HP imaging, as clinical applications to myocardial hypertrophy, failure, and infarction were obvious. An imaging sequence capable of producing multislice  $^{13}\text{C}$  images of the heart was subsequently developed and applied to porcine models, producing compelling evidence that  $^{13}\text{C}$  imaging of the heart is not only possible but also likely to be easily implemented in humans (Figure 8).<sup>115</sup> Work by others in the perfused rat heart confirmed that transient ischemia reduced PDH flux as measured by [ $^{13}\text{C}$ ]bicarbonate

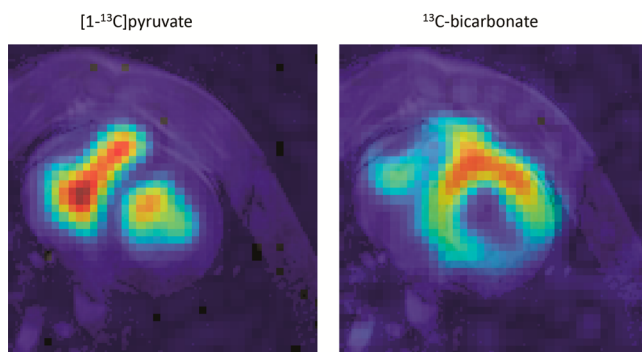


**Figure 8.** Images of porcine myocardial metabolism as imaged with HP [ $1\text{-}^{13}\text{C}$ ]pyruvate. Courtesy of A. Z. Lau and C. H. Cunningham.

production.<sup>118</sup> Furthermore, ischemia is known to cause the cytosol of the heart to become more reduced. Taking the [ $^{13}\text{C}$ ]bicarbonate/[ $1\text{-}^{13}\text{C}$ ]lactate ratio produces a metric sensitive to both these processes; it was noted that in short time periods following reperfusion the ratio increased dramatically as the heart sought to restore its energy balance. It was also noted that  $^{31}\text{P}$  spectroscopy did not have the sensitivity to detect changes in metabolism on a time scale that was the same as that of HP experiments. While [ $1\text{-}^{13}\text{C}$ ]pyruvate imaging of the heart is quite sensitive to changes in PDH flux, the generation of [ $^{13}\text{C}$ ]bicarbonate from HP [ $1\text{-}^{13}\text{C}$ ]pyruvate is not guaranteed to reflect TCA cycle turnover. HP [ $2\text{-}^{13}\text{C}$ ]pyruvate theoretically should be more sensitive to a forward turn of the cycle, as its product, acetyl-CoA labeled at the carbonyl position, can condense with oxaloacetate to produce labeled TCA cycle intermediates. This labeling scheme was used successfully by Tyler and co-workers to study the perfused heart under normal conditions and following mild ischemia.<sup>119</sup> With the injection of HP [ $2\text{-}^{13}\text{C}$ ]pyruvate, [ $1\text{-}^{13}\text{C}$ ]acetylcarnitine, [ $5\text{-}^{13}\text{C}$ ]citrate, and [ $5\text{-}^{13}\text{C}$ ]glutamate were observed, as well as the appropriate isotopomers of lactate and alanine. Ischemia-reperfusion reduced the magnitudes of the signals of the products of PDH flux, an observation interpreted as reduced TCA cycle turnover, though total pool sizes were not addressed as a possible source of the decreased magnitude of the signal. The low signal intensities associated with the [ $5\text{-}^{13}\text{C}$ ]glutamate and [ $5\text{-}^{13}\text{C}$ ]citrate do not bode well for the clinical use of HP [ $2\text{-}^{13}\text{C}$ ]pyruvate, as the sensitivity of any experiment is likely to be challenging even with hyperpolarization. Shortly thereafter, the same lab produced a dose-response study of the response of the *in vivo* rat heart to HP [ $1\text{-}^{13}\text{C}$ ]pyruvate concentration.<sup>120</sup> Injection of 1 mL of 40 mM HP [ $1\text{-}^{13}\text{C}$ ]pyruvate produced a maximal response as measured by [ $^{13}\text{C}$ ]bicarbonate production, with injections at higher concentrations producing insignificant increases. The resulting data showed Michaelis-Menten-type kinetics for PDH flux, while HP lactate and alanine production remained linear across the concentrations used. This study immediately preceded a flurry of publications by the same lab exploring the activation and control of PDH flux in a variety of systems. An *in vivo* study of PDH regulation used co-administration of malate to study the interplay between acetyl-CoA/CoA and NADH/NAD<sup>+</sup> ratios on the detected [ $^{13}\text{C}$ ]bicarbonate signal observed after injection of HP [ $1\text{-}^{13}\text{C}$ ]pyruvate.<sup>116</sup> Malate caused a 27% increase in the level of bicarbonate in the fed state, while producing insignificant changes in the fasted state, suggesting the mechanism of PDH inhibition is different between the conditions. A similar experimental design was used in a paper focused on the effects of high-fat feeding and DCA.<sup>101</sup> While significant correlations were found between PDH activity and [ $^{13}\text{C}$ ]bicarbonate generation, the best fit line did not intersect the origin. The researchers correctly pointed out that *ex vivo* assays of PDH activity could not account for other effects *in vivo*, such as product inhibition by high levels of acetyl-CoA derived from fatty acid oxidation. In a study of hyperthyroidism, the same group used both HP [ $1\text{-}^{13}\text{C}$ ]pyruvate and [ $2\text{-}^{13}\text{C}$ ]pyruvate separately to study known increases in cardiac metabolic rate.<sup>121</sup> The onset of the malady in a rat model corresponded to decreases in apparent PDH flux and an increase in pyruvate anaplerosis through pyruvate carboxylase (PC). Both acute and long-term treatment with DCA resulted in a restoration of PDH flux, increasing the metabolic flexibility of the heart and resulting in decreased hypertrophy associated

with the hyperthyroid condition. Interestingly, the use of [ $2\text{-}^{13}\text{C}$ ]pyruvate in this case allowed the observation of HP [ $3\text{-}^{13}\text{C}$ ]citrate, which can be derived only from oxaloacetate generated by PC flux followed by its condensation with acetyl-CoA. The efficacy of DCA for increasing PDH flux was studied in a different context by Mayer et al., where it was shown that an increased level of [ $^{13}\text{C}$ ]bicarbonate could be generated from HP [ $1\text{-}^{13}\text{C}$ ]lactate injected into rats.<sup>117</sup>

Pyruvate oxidation was the primary target of study in a methodological paper that for the first time used HP [ $1,2\text{-}^{13}\text{C}_2$ ]pyruvate as the imaging agent.<sup>122</sup> This agent has the unusual ability to simultaneously measure PDH flux as well as incorporation of label into the TCA cycle as it combines both of the pathways illustrated in Figure 7. While this can be translated into a tremendous gain in the amount of information from a single experiment, excellent resolution is required to capture both pathways, as the  $J$  coupling present in lactate and alanine arising from the doubly labeled pyruvate can impede the detection of [ $5\text{-}^{13}\text{C}$ ]glutamate, the most interesting downstream product of [ $2\text{-}^{13}\text{C}$ ]pyruvate. More applications of HP [ $1\text{-}^{13}\text{C}$ ]pyruvate and [ $2\text{-}^{13}\text{C}$ ]pyruvate to studies of cardiac metabolism appeared subsequently; one particularly cohesive paper studied heart failure (HF) in a porcine model.<sup>123</sup> Using an implantable pacemaker, dilated cardiomyopathy was induced by rapid pacing, with longitudinal study by cine-MRI for function,  $^{31}\text{P}$  NMR for cardiac energetics, and HP  $^{13}\text{C}$  NMR for intermediary metabolism. As seen in earlier studies, HP [ $2\text{-}^{13}\text{C}$ ]pyruvate produced signals in [ $5\text{-}^{13}\text{C}$ ]glutamate and [ $1\text{-}^{13}\text{C}$ ]acetylcarnitine, both of which decreased significantly with progression of HF. Perhaps the most encouraging result was a significant decline in the [ $5\text{-}^{13}\text{C}$ ]glutamate signal at 2 weeks of pacing that preceded any other measure of change in heart function, including cardiac index, end-diastolic volume, and ATP production as assessed by  $^{31}\text{P}$  NMR. A more comprehensive study of HP [ $1\text{-}^{13}\text{C}$ ]acetylcarnitine kinetics was conducted in the rat using DCA and dobutamine interventions.<sup>124</sup> Using saturation transfer experiments, the acetylcarnitine pool was shown to be in rapid equilibrium with both the [ $5\text{-}^{13}\text{C}$ ]citrate and [ $5\text{-}^{13}\text{C}$ ]glutamate pools. DCA administration enhanced the [ $1\text{-}^{13}\text{C}$ ]acetylcarnitine signal, consistent with increased PDH flux, while dobutamine apparently drained the acetylcarnitine pool, indicative of increased cardiac workload. Similar experiments with a larger pyruvate dose also noted changes in the [ $5\text{-}^{13}\text{C}$ ]glutamate signal and detected for the first time acetoacetate labeled at positions C1 and C3.<sup>125</sup> This was a truly remarkable result, as the heart is not believed to be a ketogenic organ. Future work should focus on the exact origin of the signal, as the large pyruvate dose could have facilitated export of ketone bodies from the liver to the heart. If the source of HP acetoacetate is truly the heart, then pathways previously considered irrelevant to the heart should be reexamined.

Up to this point, pyruvate metabolism has primarily been reviewed in the context of its oxidation or reduction, but its fate is different in the liver, which prefers to use fatty acids for oxidation, preserving three-carbon intermediates for gluconeogenesis. Liver metabolism has been less well studied in the context of hyperpolarization than cancer or myocardial metabolism. The first publication studied the *in vivo* rat liver in fed and fasted conditions.<sup>126</sup> A key observation from the data was that oxidative flux was much reduced in the liver compared to that in the heart, as [ $^{13}\text{C}$ ]bicarbonate was largely undetectable using a small flip-angle inspection pulse. As a surrogate of the redox state of the liver, the ratio of the lactate/

alanine signal was elevated, indicating a more reduced cytosol.<sup>77</sup> Given that the experiments were conducted at 3 T, where the  $^{13}\text{C}$  chemical shift resolution is limited, it is perhaps not unsurprising that data in the perfused liver collected at higher fields led to the detection of more metabolic products of [ $1\text{-}^{13}\text{C}$ ]pyruvate, including [ $1\text{-}^{13}\text{C}$ ]- or [ $4\text{-}^{13}\text{C}$ ]malate and [ $1\text{-}^{13}\text{C}$ ]- or [ $4\text{-}^{13}\text{C}$ ]aspartate.<sup>127</sup> The perfused liver also had the advantage of being placed inside a relatively small diameter (18 mm) volume coil, enhancing the sensitivity of the experimental protocol. The primary fate of pyruvate in the liver is carboxylation to form oxaloacetate, which is in rapid equilibrium with malate and fumarate. The initial carboxylation step produces only [ $1\text{-}^{13}\text{C}$ ]oxaloacetate, but fumarate is a symmetric intermediate; rapid exchange to the level of fumarate produces malate, oxaloacetate, and therefore aspartate that is labeled at both positions C1 and C4. The relative ratio of the C1 and C4 signals gives kinetic information about the rate of exchange between fumarate and the other four-carbon compounds. HP [ $^{13}\text{C}$ ]bicarbonate was also observed, the appearance of which was quenched by using a phosphoenolpyruvate carboxykinase knockout (PEPCK-KO) mouse as a control. PEPCK can compete with PDH as a source of HP [ $^{13}\text{C}$ ]bicarbonate when [ $1\text{-}^{13}\text{C}$ ]pyruvate is used as an imaging agent. *In vivo* work in the mouse liver assigned the production of [ $^{13}\text{C}$ ]bicarbonate exclusively to PDH flux without further proof.<sup>128</sup> This apparent disconnect led to further experiments in the *in vivo* rat liver, which favored the interpretation that PDH flux is primarily responsible for HP [ $^{13}\text{C}$ ]bicarbonate production *in vivo*.<sup>129</sup> It is likely that the use of the medium-chain fatty acid octanoate, which bypasses carnitine palmitoyl transferase-I (CPT-I), in the perfused livers resulted in high levels of acetyl-CoA and a concomitant drop in PDH flux due to product inhibition. In all cases in which the chemical shift resolution is sufficient, the equilibrium products of oxaloacetate have signal amplitudes larger than those of [ $^{13}\text{C}$ ]bicarbonate, indicating that PC flux is larger in the liver than PDH flux.

## ■ KINETICS

Central to the appeal of hyperpolarization for metabolic imaging is the capture of time-resolved kinetics that reflects flux through enzyme-catalyzed reactions. As evidenced in the preceding text, tremendous progress has been made using rudimentary but highly stable ratios of metabolites to their HP precursors. The most intellectually satisfying solution to the reduction of HP data would fit the time-dependent evolution of the metabolites, thereby extracting rate constants and flux values for the enzyme-catalyzed reactions. This goal has been the target of multiple publications spanning a variety of systems from simple spectroscopy in cell culture to *in vivo* imaging experiments. The kinetics of HP signals is complicated by multiple factors, primarily relating to accounting for the disappearance of the HP magnetization.  $T_1$  destroys the HP magnetization at a predictable rate, but the mathematics describing first-order reaction rates is identical to that of longitudinal relaxation. This results in the superposition of exponentials with similar decay constants; extraction of decay rate constants in this case is well-known as being computationally difficult. Furthermore, each excitation of the magnetization consumes a portion of the polarization. While this factor can be exactly modeled, uncertainty about flip angles in the active volume of the transmit coil adds a further layer of uncertainty to the simulations of the data.<sup>130</sup> Other

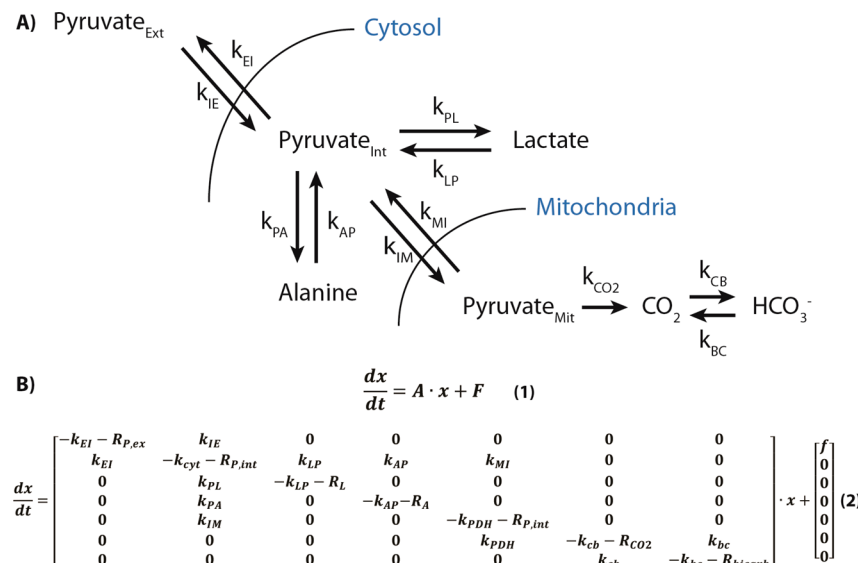


**Figure 9.** (A) Model of pyruvate metabolism including compartmentalization and enzyme-catalyzed reactions. (B1) Generalized solution for the time evolution of the signals in an HP pyruvate experiment. (B2)  $R_x$  refers to a longitudinal relaxation rate for the metabolite, and  $k_{cyt} = k_{PL} + k_{PA} + k_{IM} - k_{LP} - k_{AP}$ . The rate constant,  $k$ , is defined for each reaction or transport step. Abbreviations:  $k_{EI}$ , extracellular to intracellular;  $k_{IM}$ , intracellular to mitochondrial;  $k_{PL}$ , pyruvate to lactate;  $k_{PA}$ , pyruvate to alanine;  $k_{CO2}$ , production of  $\text{CO}_2$  following PDH flux;  $k_{CB}$ , production of bicarbonate following forward flux of  $\text{CO}_2$  through carbonic anhydrase.

considerations make the inference of exact rate constants difficult at best.

The primary experimental issue is accounting for the delivery of the HP substrate to the site of the reaction. Without the concentration of the substrate being measured, any rate constant derived from a fitting procedure per force yields only an apparent rate constant ( $k_{app}$ ). Additionally, any reaction rate measured by the appearance of a product must represent a sum of transport phenomena and the action of the enzyme, unless the intra- and extracellular fractions can be resolved in some manner. Nonetheless, extensive efforts by multiple laboratories have yielded compelling results. To facilitate a more cohesive discussion of the modeling, Figure 9 illustrates the reaction pathways of pyruvate with the attendant nomenclature of the relevant rate constants. All discussion of modeling in this paper uses this nomenclature to describe the metabolic pathways as opposed to that used in any individual paper. Equation B1 shows a matrix formulation for the differential equations that govern the time evolution of the detected signal. The matrix formulation allows an intuitive visualization of the reactions relevant to the system, as off-diagonal components describe the rate of flow from one pool to the other. The vector  $[x]$  is a column vector with an entry for each compartment and/or metabolite;  $A$  is an exchange matrix, and  $F$  is a column vector with an entry  $f$  that can be any function that accurately describes the arrival of pyruvate at the region being examined. Computationally, the solution of eq 2 involves a matrix inversion that is notably faster than any numerical methods for integrating the differential equations themselves. The resulting gain in speed results in much faster simulations in the context of fitting acquired data.

Foundational observations were reported by the Brindle lab in 2007 in an EL-4 cancer cell culture, with experiments subsequently generalized to an orthotopic tumor model.<sup>79</sup> Using the two-pool modified Bloch equations to describe only pyruvate and lactate, an apparent rate constant was extracted for LDH in culture. Furthermore, reverse flux from lactate to

pyruvate was neglected. Using a known amount of pyruvate,  $k_{PL}$  was used to calculate a flux in units of nanomoles per second per  $10^8$  cells. Treatment of the cells with etoposide reduced the measured flux significantly. From the perspective of kinetic measurements, perhaps the most important observation was that addition of exogenous lactate at concentrations of 20 and 40 mM to the cell culture resulted in 1.4- and 2.4-fold increases, respectively, in the apparent flux from pyruvate to lactate. As accurately described in the paper, this effect reflects the exchange between pyruvate and lactate that is mediated by the bidirectional LDH enzyme. A larger pool of lactate is more capable of accepting the HP  $^{13}\text{C}$  label while returning to the pyruvate pool only the unpolarized  $^{12}\text{C}$  lactate. A larger pool size exchanging with the source of HP magnetization will record a signal that is larger than that arising from a smaller pool. While CSI experiments were used to produce color maps of tumor metabolism, the *in vivo* kinetic data were collected with a slice-selective spectroscopy protocol. In the current literature, this is the case more often than not, as the development of fast imaging sequences that can be used for quantitative kinetic studies is challenging. Not only do pulse flip-angle effects have to be accurately accounted for, but sampling of  $k$ -space and general imaging considerations require sophisticated approaches to pulse sequence design.<sup>131</sup> To avoid the problem of delivery, the *in vivo* data were fit for time points only after the lactate signal had reached a maximum. This removes the need to model the delivery, but it is not clear how this compromise affects the estimation of  $k_{PL}$ . Another paper of fundamental importance carefully studied the apparent Michaelis–Menten kinetics of HP pyruvate metabolism in rats and TRAMP mice.<sup>132</sup> Rats were studied using increasing concentrations of HP pyruvate to construct the dose–response curves. Using a slice-selective detection protocol, HP pyruvate arrival and subsequent metabolism were modeled using a piecewise description of the kinetics. In addition, consumption of magnetization by the finite excitation pulses was also modeled, allowing estimates of *in vivo*  $T_1$  values of the

metabolites to be made. Again, the flux of lactate to pyruvate was neglected to simplify the fitting procedure, and modeling of the effects of the MCTs was not included in the simulations. The apparent  $V_{max}$  and  $K_m$  for the pyruvate to lactate conversion were  $11.12 \pm 1.28 \mu\text{mol kg}^{-1} \text{s}^{-1}$  and  $160 \pm 30 \mu\text{mol/kg}$ , respectively. Alanine had an almost equivalent  $V_{max}$  but the apparent  $K_m$  was larger ( $280 \pm 67 \mu\text{mol/kg}$ ). Initial velocities of each reaction were also calculated. In the TRAMP model, the ratio of apparent  $k_{PL}$  to  $k_{PA}$  increased over time in animals that were untreated, but hormone deprivation therapy prevented this rise, suggesting that quantitatively accounting for reaction rates might provide a stable metric for assessing treatment efficacy and tumor progression. An important observation in the study was that the measured  $T_1$  values of pyruvate, lactate, and alanine depended upon the tissue in which they were observed. One of the most complete attempts to assess *in vivo* kinetics using a Michaelis–Menten model was undertaken in the rat kidney.<sup>133</sup> In this case, an external reference was added to help estimate the total pyruvate concentration at the site of imaging. Using this method,  $V_{max}$  and  $K_m$  values were estimated for the production of HP lactate and alanine. The authors demonstrated that under the appropriate infusion conditions, the size of the pyruvate bolus (1, 2, or 3 mL) did not compromise estimates of the Michaelis–Menten constants. This observation deserves to be reproduced in other laboratories. If their method of kinetic analysis is shown to be sufficiently robust, it would allow discussion of *in vivo* kinetics in general terms understood by any scientific field, enhancing the likelihood of collaborations between the basic science groups driving the technology and more applied medical research teams.

Taking a step back in biological complexity, but a step forward in the complexity of the modeling, Harris et al. studied a T47D cell culture model of human breast cancer using a perfusion rig placed in a vertical bore spectroscopy system.<sup>134</sup> In this case, pyruvate extra- to intracellular transport was modeled in addition to pyruvate to lactate flux. One of the primary advantages of cell culture systems for measuring kinetics is that pyruvate delivery can accurately be approximated by a Heaviside step function, with only subsequent metabolism resulting in a change in pyruvate concentration. The addition of an MCT1 inhibitor to the system caused large drops in the HP lactate signal, as did a washout protocol that rapidly removed the HP pyruvate bolus. The combination of these two methods allowed the authors to state that pyruvate extra- to intracellular transport was the primary site of control of the total HP lactate signal, though generalizing this conclusion to other situations should be done with circumspection. Using a similar perfusion system, Keshari et al. studied an immortalized hepatoma cell line using HP pyruvate but arrived at different conclusions about the minimal model needed to describe the system.<sup>135</sup> Experimentally, the data were acquired in a manner different from that of Harris et al., who used a stopped flow technique. Here the system was under constant perfusion, and therefore, the data were modeled using an exponential delivery function. Using a 5° nonselective pulse, both lactate and alanine were observed and the resulting data were fit to derive  $k_{PL}$  and  $k_{PA}$  values without reference to MCT function. Despite the divergence in the choice of model, the ultimate fluxes estimated by the two methods were within 1 order of magnitude of each other. A third lab studied similar questions of MCT versus LDH activity in the EL4 cancer cell line, concluding that both MCT and LDH were responsible for

controlling the intensity of the lactate signal.<sup>136</sup> As detailed above, the majority of studies have approached the modeling problem assuming unidirectional flux. While this certainly appears to be a reasonable simplification of the modeling, data demonstrating that exchange has a negligible effect on the observed kinetics were scant. Using SF188-derived glioblastoma cells in suspension in an NMR tube, Harrison and co-workers proposed six models of pyruvate metabolism that included exchange, flux, and separate pools of intra- and extracellular lactate.<sup>137</sup> Previously, independent measures of  $^{13}\text{C}$  isotope distribution had not been included in the experimental protocol, but here for the first time, mass spectrometry was used to independently assess  $^{13}\text{C}$  enrichment of the lactate pool. The experimental design included parallel experiments with [ $3-^{13}\text{C}$ ]pyruvate in cells that could be rapidly frozen to arrest metabolism; three time points at short, intermediate, and long times after introduction of pyruvate were used as gold standards for flux and/or exchange between pyruvate and lactate. To boost the NMR sensitivity further, a shaped pulse protocol was used to provide minimal excitation for the pyruvate while using an 18° flip angle for the [ $1-^{13}\text{C}$ ]lactate signal. As one might expect, only exchange models could fit the mass spectrometry and HP data simultaneously, with the three-pool bidirectional exchange model producing the fit with the lowest residuals overall. Remarkably, most models produced an accurate estimate of the initial pyruvate to lactate reaction as measured via hyperpolarization. The key point of this observation is that due to the shortness of time that the HP signal is observed, rather simple approximations can yield quantitative estimates of metabolic flux when using simple excitation–detection protocols. All four of these papers that used cell culture as a model system produced estimates of pyruvate to lactate flux ( $V_0$ ) that were within 1 order of magnitude, probably well within the biological variability of the various tumor cell lines used. Oxidative metabolism is also active in cancer cells, as detected using HP [ $1-^{13}\text{C}$ ]pyruvate in cell culture.<sup>138</sup> Using a selective excitation pulse to amplify the observed [ $^{13}\text{C}$ ]bicarbonate signal, kinetics in two different cancer cell lines were studied. The SFxL cell line primarily oxidizes pyruvate, as opposed to the hepatocellular carcinoma cell line, Huh-7, which metabolizes pyruvate more avidly via anaplerosis. The exact cell count along with a known volume and concentration of injected HP pyruvate facilitated an absolute measure of PDH flux, which could then be used to assign quantitative fluxes to a network of reactions probed by steady-state isotopomer analysis.

The conclusion that exchange is not important for accurate estimates of initial flux stands in apparent contradiction to methods that use more sophisticated pulse sequences to encode metabolic information into the HP data. Magnetization transfer experiments used to study *in vivo* cancer metabolism demonstrated the necessity of modeling bidirectional flux in an orthotopic tumor model.<sup>139</sup> In this experiment, after injection of the HP pyruvate, signals from pyruvate or lactate were irradiated for 1 s, producing changes in the signal intensity for the exchanging peak. These experiments parallel the MAD-STEAM method for *in vivo* spectroscopy, which uses specific echo times in a stimulated echo experiment to measure the change in phase of signal that arises when exchange takes place.<sup>140</sup> In both these experiments, bidirectional exchange is easily detected, even if estimates of flux are complicated by a lack of quantitative estimates of HP pyruvate concentration at the tumor. The key to understanding the disconnect between

these experiments and those performed in cell culture is the preliminary encoding of the magnetization (either through saturation or by relative frequency) prior to its detection. The resulting  $k$  values are measures of exchange throughout the experiment as opposed to the initial velocity,  $V_0$ , that is measured in the cell culture models. Determination of which methods yield the best insights into the biological process that is being studied is up to the designer of the experiment. The desire to accurately model exchange *in vivo* has recently prompted thoughtful development of phantoms for use in horizontal bore imaging systems.<sup>141</sup> Future development of imaging sequences would benefit from a uniform standard such as the one proposed by Walker et al. in benchmarking results from multiple laboratories concurrently. Another alternate method for assessing label exchange between lactate and pyruvate uses both HP [1-<sup>13</sup>C]pyruvate and HP [1-<sup>13</sup>C]lactate that is specifically deuterated. Using a pulse sequence similar to that of the POCE experiment,<sup>142</sup> the intensity of the free induction decay versus the echo can be used to detect exchange.

## FATTY ACID AND KETONE METABOLISM

Long-chain fatty acids (LCFAs) and ketones are preferentially oxidized in the majority of the organs, as the body ideally reserves glucose for utilization by the brain. Fatty acid  $\beta$ -oxidation is a large source of reducing equivalents as well as acetyl-CoA, but a technical factor has completely stopped the development of LCFAs as imaging agents, namely the fact that they require albumin to be solubilized in water. Albumin is a large, slowly tumbling molecule that has a strong negative impact on the <sup>13</sup>C  $T_1$  values of the LCFAs when the compounds are complexed together, essentially depolarizing the agent upon binding. Water-soluble short-chain fatty acids like butyrate seem like obvious targets for development, so it is somewhat surprising that the first published results with butyrate are relatively new.<sup>143</sup> Initially using a perfused heart model, the injected HP [1-<sup>13</sup>C]butyrate was rapidly metabolized to [1-<sup>13</sup>C]acetoacetate, [1-<sup>13</sup>C]- $\beta$ -hydroxybutyrate, [1-<sup>13</sup>C]acetylcarnitine, [S-<sup>13</sup>C]citrate, and [S-<sup>13</sup>C]glutamate. It is of note that [1-<sup>13</sup>C]butyrate produces the same isotopomers as [2-<sup>13</sup>C]pyruvate, but the additional information gained from the observation of the ketone bodies is a significant enhancement of the available information. The heart is generally not considered a ketogenic organ, yet a process known as pseudoketogenesis is known to be active in muscle/heart tissue.<sup>144</sup> This process, a subject of much contention in the literature, uses circulating acetoacetate to exchange with acetoacetyl-CoA in a process that redistributes the <sup>13</sup>C label without actually producing new ketone bodies. Experiments with HP [1-<sup>13</sup>C]butyrate *in vivo* were also quite successful in the same study, though the spectral resolution is lower compared to that in the perfused heart. As detailed in the section on [2-<sup>13</sup>C]pyruvate, the production of [1-<sup>13</sup>C]acetylcarnitine can also be interpreted as a readout of the energy state of the myocardium; higher acetylcarnitine levels indicate a greater energy reserve available for the heart.

Acetate is not strictly a fatty acid, but it is the smallest two-carbon precursor to acetyl-CoA and is avidly metabolized by a number of tissues. As an imaging agent, HP [1-<sup>13</sup>C]acetate was first discussed by Jensen et al. in the context of heart and skeletal muscle metabolism *in vivo*.<sup>145</sup> Under an ischemia-reperfusion protocol, the signal associated with [1-<sup>13</sup>C]acetylcarnitine was dramatically lower during ischemia and

was significantly depressed with even a 1 h reperfusion of the hindlimb. Unfortunately, because of the chemical shift of the parent [1-<sup>13</sup>C]acetate molecule, it is surprisingly difficult to resolve the [S-<sup>13</sup>C]glutamate signal that should be derived from exchange between  $\alpha$ -ketoglutarate and glutamate. Mishkovsky et al. have demonstrated that by using uniformly <sup>13</sup>C-enriched acetate and a polarization transfer pulse sequence, the metabolism of acetate to the level of  $\alpha$ -ketoglutarate can be detected in the rat brain.<sup>64</sup> It was very surprising that  $\alpha$ -ketoglutarate could be detected, as it is typically present at concentrations much lower than that of glutamate in the brain. The same group subsequently conducted a thorough kinetic analysis of [1-<sup>13</sup>C]acetate and its appearance in [1-<sup>13</sup>C]-acetylcarnitine in the muscle, as well.<sup>146</sup>

Ketone bodies themselves have long  $T_1$  carbonyls that should be amenable to hyperpolarization studies. To date, no papers have been published using HP acetoacetate or  $\beta$ -hydroxybutyrate as an imaging agent, but these compounds are clearly on the mind of many researchers as evidenced by two abstracts presented at a recent meeting.<sup>147,148</sup> Given the rapid uptake of ketone bodies by the brain and heart during fasting, it would be surprising if compelling *in vivo* results were not forthcoming.

As a conclusion to this portion of the review, truly original insights into *in vivo* oxidative metabolism are now being generated using dissolution DNP and a variety of <sup>13</sup>C-labeled precursors. The incredible specificity of MR allows the observation of kinetics in real time in a straightforward manner unmatched by other molecular imaging techniques. This section has outlined how the redox state of the cell is important in both cancer and normal physiology. The lactate–pyruvate equilibrium has long been an important target for measurement, but the NAD<sup>+</sup>/NADH ratio on which it reports should not be confused with the NADPH-mediated detoxification processes that are also a part of normal cell function. This pool of redox active metabolites is reviewed in the next section.

## OXIDATIVE STRESS: VITAMIN C AND ITS REGENERATION

As mentioned above, ROS play a central role in many normal cellular processes, including intracellular signaling and mitochondrial electron transport, but an excessive concentration of ROS lead to oxidative stress and may cause cell damage.<sup>149</sup> Antioxidants such as ascorbate (Asc or vitamin C) are essential in maintaining intracellular and extracellular redox homeostasis, and the extent of their usage increases in the case of oxidative stress. Through the ROS-scavenging process, ascorbate is oxidized to dehydroascorbate (DHA), the membrane transport of which is facilitated by the GLUT protein family, making DHA the prevalent form for cells to incorporate vitamin C.<sup>150</sup> As soon as DHA enters cells, it is nearly instantaneously reduced to ascorbate via processes that can involve several reductants, allowing vitamin C recycling, as detailed below, but before entering the cell, DHA can also be hydrolyzed to diketogulonate (DKG). The *in vivo* formation of DKG from DHA is thought to be an extracellular irreversible reaction that will prevent part of the DHA from being reduced to vitamin C, although this point seems to be controversial.<sup>151</sup> The recycling of DHA to vitamin C is a crucial step in the maintenance of cellular redox balance.

The idea proposed essentially at the same time by Keshari et al. and Bohndiek et al. is to hyperpolarize and inject solutions containing [1-<sup>13</sup>C]DHA to probe the intracellular redox status

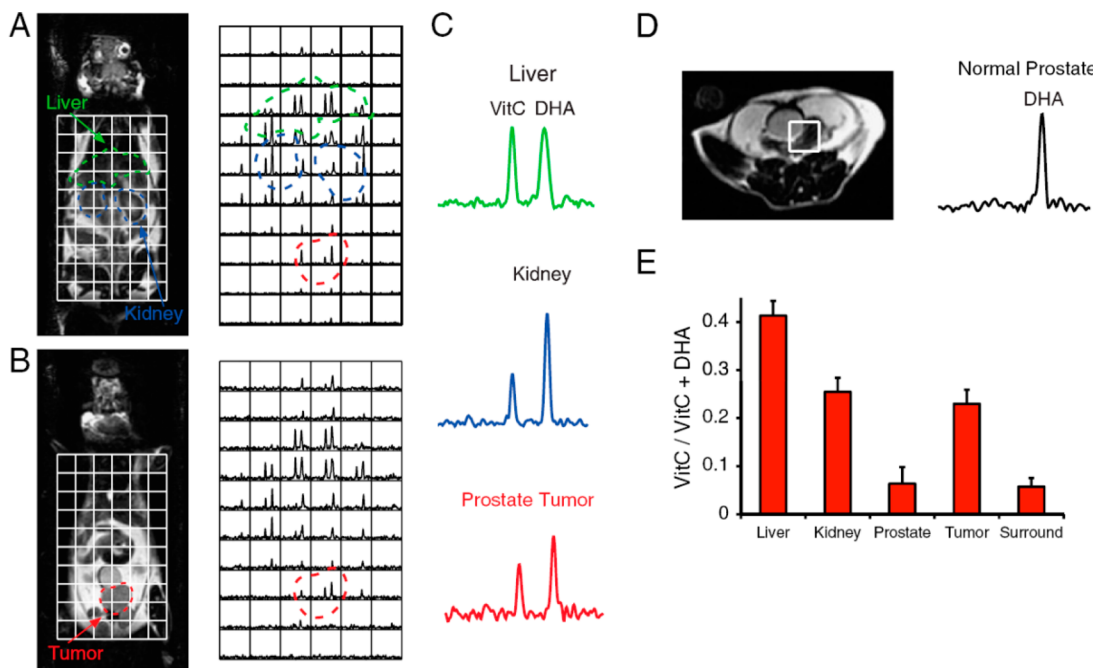


**Figure 10.** (A and B) Sequential coronal  $T_2$ -weighted images and corresponding  $^{13}\text{C}$  three-dimensional MRSI demonstrating the distribution of HP DHA and vitamin C (VitC) in a TRAMP mouse after intravenous injection of  $350\ \mu\text{L}$  of  $15\text{ mM}$  HP [ $1-^{13}\text{C}$ ]DHA. The liver and kidneys are best seen in panel A, and the prostate tumor is best seen in panel B. (C) Representative  $^{13}\text{C}$  spectra from liver, kidney, and prostate tumor in a TRAMP mouse. (D) Axial  $T_2$ -weighted image of a normal mouse with a voxel encompassing the normal prostate. (E) Summary of average metabolite ratios [VitC/(VitC + DHA)] for normal liver, kidneys, and prostate ( $n = 5$ ), as well as TRAMP tumor and surrounding benign tissue (surround) ( $n = 4$ ). Reproduced with permission from ref 153. Copyright 2011 National Academy of Sciences.

by measuring the  $^{13}\text{C}$  NMR signal intensity ratio between [ $1-^{13}\text{C}$ ]DHA and [ $1-^{13}\text{C}$ ]Asc.<sup>152,153</sup> The properties of these two compounds are indeed very attractive for HP  $^{13}\text{C}$  NMR measurements because the C1 of each compound has a relatively long  $T_1$ , especially at moderate and clinically compatible magnetic fields, and their chemical shift difference is large enough to be easily distinguished (Figure 10). The attractiveness of DHA as a HP probe might, however, be hindered by its relative acute toxicity (the LD<sub>50</sub> of rats with unbuffered iv DHA is  $\sim 0.32\text{ g/kg}$ ),<sup>154</sup> and to a lesser extent its tendency to be hydrolyzed to DKG.

An additional significant issue for biological applications of HP [ $1-^{13}\text{C}$ ]DHA lies in the difficulty of interpreting the origin of the  $^{13}\text{C}$  NMR signal intensity ratio inherent to the intricate reduction mechanisms. Reduction of DHA to vitamin C can be either spontaneous, through a reaction with glutathione (GSH), another major intracellular antioxidant, or enzymatically catalyzed with the direct or indirect involvement of NADPH (Figure 11). GSH, which unlike vitamin C can be directly synthesized by human (and many other mammalian) cells, is also involved in the most prominent reduction pathway via a thiol cycle (Figure 11B). The concentration ratio of glutathione disulfide (GSSG) to GSH, namely [GSSG]/[GSH], has been determined to be a direct indicator of oxidative stress.<sup>155</sup> For this reason, and because of the high intracellular concentration of GSH (ranging from  $0.5$  to  $10\text{ mM}$ ), it is tempting to hypothesize that the [ $1-^{13}\text{C}$ ]DHA to [ $1-^{13}\text{C}$ ]Asc intensity ratio should correlate with [GSSG]/[GSH]. However, one has to be cautious because, first, GSH-independent processes that depend on NADPH can directly reduce DHA (Figure 11A), for instance, via the thioredoxin reductase,<sup>156</sup> or  $3\alpha$ -hydroxysteroid dehydrogenase,<sup>157</sup> and, second, the concentration of NADPH could be the rate-limiting factor, even with

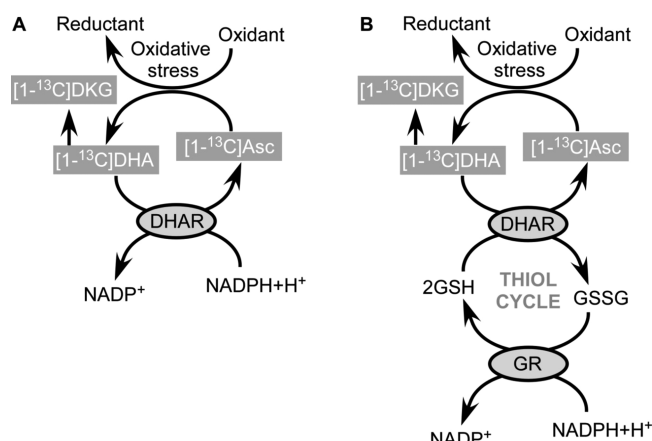


**Figure 11.** Schematic representation of the enzymatically catalyzed DHA reduction processes. The cofactor NADPH is involved either directly (A) or via a thiol cycle (B). The most prominent thiol cycle couples the reduction of DHA to the oxidation of glutathione, the recycling (reduction) of which involves the oxidation of NADPH. Abbreviations: DHAR, dehydroascorbate reductase; GR, glutathione reductase.

the involvement of GSH, because it is required to reduce GSSG through glutathione reductase (GR). It must also be noted that three different types of GSH-dependent enzymes have been shown to have dehydroascorbate reductase (DHAR) activity, namely, thioltransferases (also known as glutaredoxins), glutathione S-transferases, and protein disulfide isomerase.<sup>158,159</sup>

Despite its limitations, [ $1-^{13}\text{C}$ ]DHA is the only HP substrate for probing the intracellular NADPH availability *in vivo* that has been proposed to date, and it can provide crucial information in

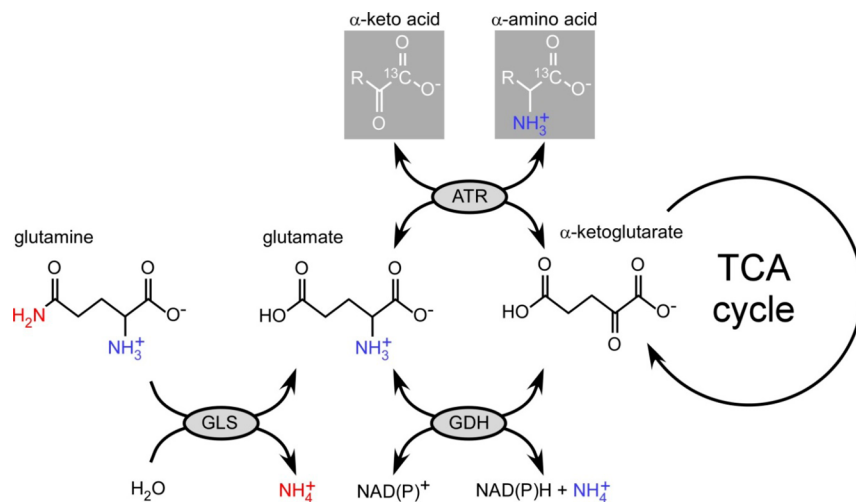


**Figure 12.** Schematic representation of the transamination and transamidation reactions involving glutamate. Abbreviations: GLS, glutaminase; ATR, aminotransferase; GDH, glutamate dehydrogenase.

ROS-related diseased tissue, in particular for clinically relevant cardiovascular and neurodegenerative diseases as well as cancer. So far, the only two published studies based on HP [ $1^{13}\text{C}$ ]DHA have been performed in tumor models.<sup>152,153</sup> The fast proliferation of cancer cells is associated with an increased concentration of ROS, which is partly compensated by an increase in intracellular antioxidant concentration, principally GSH and NAPDH from the upregulated pentose phosphate pathway.<sup>160,161</sup> There is therefore a direct relationship between the concentration of reducing molecules and tumor cell development, and HP [ $1^{13}\text{C}$ ]DHA could provide an assessment of the aggressiveness of cancer cells and their response to drugs.

## ■ AMINO ACID METABOLISM AND NITROGEN HOMEOSTASIS

Nitrogen homeostasis is tightly regulated in animals, on one hand, because of the nitrogen requirements in essential processes such as nucleic acid and protein synthesis and neurotransmission and, on the other, because of the high toxicity of ammonia. Nitrogen is assimilated by the organism through the diet in the form of nucleotides, proteins, and amino acids. The release (deamination) or intermolecular transfer (transamination) of an amino group is an essential enzymatically catalyzed process in the metabolism of amino acids.<sup>162</sup> Among the TCA cycle intermediates connecting the glucogenic amino acids to carbohydrate metabolites, two  $\alpha$ -keto acids, namely,  $\alpha$ -ketoglutarate ( $\alpha\text{-KG}$  or 2-oxoglutarate) and oxaloacetate, are key molecules because they participate in the transfer of reducing equivalents between the cytosol and the mitochondrion to regulate metabolism and in particular oxidative phosphorylation. This transfer via the malate–aspartate shuttle involves the two associated amino acids aspartate and glutamate. The latter, participating in several transamination reactions and functioning as both a nitrogen acceptor and a nitrogen donor, plays a prominent role in the intracellular transport of nitrogen as well as in biosynthesis (Figure 12).

Several HP probes have been proposed and tested to detect the metabolism of these key compounds in amino acid metabolism and their associated pathways. To date, applications in oncology and neurosciences have been proposed, and we

review here the probes within their potential fields of application.

**Cancer Metabolism.** Because it has been shown that glutamine is, along with glucose and lactate, a major fuel for the proliferation of tumor cells, HP [ $1^{13}\text{C}$ ]glutamine was evaluated to probe cancer metabolism. Early *in vitro* experiments by Gallagher et al. showed that [ $5^{13}\text{C}$ ]glutamate can be readily detected in cultured human hepatoma cells (HepG2) following the injection of HP [ $5^{13}\text{C}$ ]glutamine into cell suspensions and that the rate of conversion is determined by both the glutaminase (GLS) activity and the kinetics of the glutamine transporters.<sup>163</sup> Cabella et al. later showed that similar HP  $^{13}\text{C}$  experiments can be performed *in vivo* in rat liver injected with rat hepatoma cells (McA-RH7777).<sup>164</sup> Although the  $T_1$  and chemical shift of both the [ $5^{13}\text{C}$ ]glutamine precursor and the [ $5^{13}\text{C}$ ]glutamate metabolite are suitable for hyperpolarization, the challenges associated with such an experiment have two main origins. First, glutamine is quite unstable in aqueous solution and tends to be converted to [ $5^{13}\text{C}$ ]pyroglutamate.<sup>164</sup> Second, the cellular uptake of glutamine is relatively slow, even in cancer cells [typically  $2\text{--}3 \text{ nmol min}^{-1} (\text{mg of protein})^{-1}$  (see, e.g., ref 165)]. Note that although [ $1^{13}\text{C}$ ]glutamine has a  $^{13}\text{C}$   $T_1$  longer than that of [ $5^{13}\text{C}$ ]glutamine because of the larger intramolecular distance between the  $^{13}\text{C}$  label and a quadrupolar  $^{14}\text{N}$  atom, the small chemical shift difference between [ $1^{13}\text{C}$ ]glutamine and [ $1^{13}\text{C}$ ]glutamate makes it less suitable for *in vivo* experiments.

The transamination of glutamate to  $\alpha$ -ketoglutarate can be probed using HP [ $1^{13}\text{C}$ ]glutamate and has been demonstrated *in vitro* in human hepatoma cells (HepG2).<sup>166</sup> This probe is also attractive in tumors because of the high intracellular glutamate concentration resulting from the high rate of glutamine uptake and glutaminase activity that has been reported in cancer cells.<sup>167</sup> In addition, the labeling of [ $1^{13}\text{C}$ ]- $\alpha$ -ketoglutarate could give access to the measurement of oncogenic hypoxia-inducible factor (HIF) pathways that have been recently discovered.<sup>168</sup> In fact, [ $1^{13}\text{C}$ ]- $\alpha$ -ketoglutarate has been recently proposed as a HP probe to assess the IDH1 mutational status in glioma.<sup>169</sup> The transfer of the  $^{13}\text{C}$  from [ $1^{13}\text{C}$ ]- $\alpha$ -ketoglutarate to [ $1^{13}\text{C}$ ]-2-hydroxyglutarate was detectable only in tumor cells expressing mutant IDH1. One of the main challenges for further applications of this probe will be

the relatively weak signal of [ $1^{13}\text{C}$ ]-2-hydroxyglutarate coupled to the fact that it overlaps with the signal from [ $5^{13}\text{C}$ ]- $\alpha$ -ketoglutarate (the chemical shift difference is only 0.1 ppm), which is present at natural abundance but is also HP and thus gives rise to a detectable signal.

Besides pyruvate, which is converted to alanine, the other  $\alpha$ -keto acid coupled to the glutamate- $\alpha$ -ketoglutarate transamination reaction that has been proposed as an HP probe is  $\alpha$ -ketoisocaproate (KIC). KIC, along with the other two branched-chain  $\alpha$ -keto acids (BCKAs), namely,  $\alpha$ -keto- $\beta$ -methylvalerate and  $\alpha$ -ketoisovalerate, transforms into a branched-chain amino acid (BCAA) following the incorporation of the amino group from glutamate (see Figure 12). Leucine is associated with KIC, isoleucine with  $\alpha$ -keto- $\beta$ -methylvalerate, and valine with  $\alpha$ -ketoisovalerate. Karlsson et al. demonstrated that the intensity of the [ $1^{13}\text{C}$ ]leucine signal intensity following the injection of [ $1^{13}\text{C}$ ]KIC in a rat lymphoma model correlates with the activity of the branched-chain aminotransferase (BCAT) (Figure 13).<sup>170</sup> The glutamate

brain glutamate.<sup>7</sup> Although no glutamate was initially detected in the rat brain following the injection of HP [ $2^{13}\text{C}$ ]-pyruvate,<sup>171</sup> HP  $^{13}\text{C}$  had the promise of offering the possibility of directly measuring metabolic intermediates involved in cerebral metabolism. Perhaps one of the most remarkable observations obtained with HP  $^{13}\text{C}$  in terms of brain metabolism was the detection of [ $5^{13}\text{C}$ ]- $\alpha$ -ketoglutarate from [ $1^{13}\text{C}$ ]acetate and the absence of a [ $5^{13}\text{C}$ ]glutamate signal within the 30 s time frame of the experiment.<sup>64</sup> Interestingly, Park et al. detected [ $5^{13}\text{C}$ ]glutamate but no [ $5^{13}\text{C}$ ]- $\alpha$ -ketoglutarate in the rat brain following the injection of HP [ $2^{13}\text{C}$ ]pyruvate.<sup>172</sup> This difference might be due to the fact that acetate is exclusively taken up by astrocytes whereas pyruvate is most likely incorporated in both neurons and astrocytes.

The essential glutamate/glutamine cycle sustains the formation of the glutamate neurotransmitter within neurons while preventing its superfluous and toxic accumulation within the synaptic cleft. Because both glutamate and glutamine can be oxidized, the brain requires an abundant source of amino groups for synthesizing these vital amino acids. BCAAs and notably leucine are known to be a major source of nitrogen for the synthesis of glutamate and glutamine, and Yudkoff et al. hypothesized that BCAAs should play a crucial role in the recycling of glutamine in astrocytes and the buffering of glutamate within neurons (see Figure 14).<sup>173</sup> Experimental evidence of the role of BCAAs in *de novo* glutamate synthesis and glutamate recycling via a BCAA shuttle was provided by Hutson et al.<sup>174</sup> Together with the high level of expression of BCAT in the rodent and human brain,<sup>175</sup> the facilitated transport of BCKAs through the ubiquitous cerebral MCTs makes HP [ $1^{13}\text{C}$ ]KIC an ideal compound for probing nitrogen homeostasis in the brain, and Butt et al. demonstrated that its metabolic product [ $1^{13}\text{C}$ ]leucine can be readily detected in the rat brain.<sup>176</sup> A potential application of this HP compound would be to probe the dysfunctions in amino acid metabolism linked to neurodegenerative diseases.<sup>177</sup>

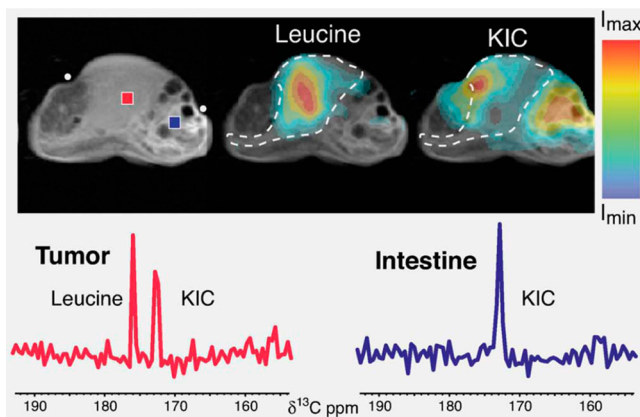


**Figure 13.** Imaging of BCAT activity *in vivo*. The anatomical  $^1\text{H}$  image of an EL4 mouse is shown at the top left. Chemical shift images of [ $1^{13}\text{C}$ ]leucine and [ $1^{13}\text{C}$ ]KIC after injection of HP [ $1^{13}\text{C}$ ]KIC are overlaid onto the anatomical image. The tumor position is indicated by a dashed line. [ $1^{13}\text{C}$ ]Leucine is specifically observed inside the tumor. One-dimensional  $^{13}\text{C}$  spectra for volume elements of the tumor and intestine (blue and red dots) demonstrate the difference in the [ $1^{13}\text{C}$ ]leucine signal between the tumor and surrounding tissue. The position of the surface coil is indicated by the two white dots at the top left. Reproduced with permission from ref 170. Copyright 2009 UICC.

pool size also plays an important role in the conversion of [ $1^{13}\text{C}$ ]KIC to [ $1^{13}\text{C}$ ]leucine because the  $K_m$  of BCAT for glutamate is  $\sim$ 50-fold larger than for KIC. As the glutamate concentration tends to be high in tumor tissue, it could be expected that the probe has a poor specificity and cannot be used to distinguish between different types of tumors. However, the authors nicely demonstrated that because BCAT is upregulated in specific cancer cells only, HP [ $1^{13}\text{C}$ ]KIC can be used as a probe for tumor profiling. While the reviewers believe that this compound might be one of the most clinically viable HP probes for applications in oncology suggested to date, no other studies have been published since this initial application in subcutaneous tumors.

**Brain Metabolism.** Because glutamate is the main excitatory neurotransmitter in the central nervous system (CNS), many *in vivo* thermally polarized NMR studies have been performed to examine how the  $^{13}\text{C}$  from [ $^{13}\text{C}$ ]glucose, [ $^{13}\text{C}$ ]acetate, or [ $^{13}\text{C}$ ]- $\beta$ -hydroxybutyrate is incorporated into

## FUTURE PROSPECTS FOR ANALYTICAL APPLICATIONS

In view of the physical considerations presented in the first part of this review, we now propose to discuss what the features of an ideal hyperpolarizer for preclinical experiments should be. First, it should be clear from Figure 1 that the working temperature has to be close to 1 K; i.e., the sample should be placed in superfluid liquid helium, although we recommend to stay above 1 K because of the prohibitively long polarization buildup time constants. Also, because the amount of microwave power required for efficient DNP is non-negligible (typically 10–50 mW), the sample cannot be placed in a vacuum chamber while being cooled by a cryogenic cold head and should instead be immersed in superfluid liquid helium. However, because of the scarcity as well as the cost of helium, we advocate for a system that will not require external cryogenic fluids. The idea would thus be to have a small amount of condensed helium inside the sample space that can be internally recycled (this is what is actually done in the SPINlab). Second, as discussed earlier, the most convenient magnetic field seems to be 5 T (the current version of SPINlab is also set to operate at 5 T). Third, the sample volume and dilution factor should be small, so that it is possible to produce adapted volumes of highly concentrated solutions for cell cultures (in 5 or 10 mm outer diameter NMR tubes) or rodents

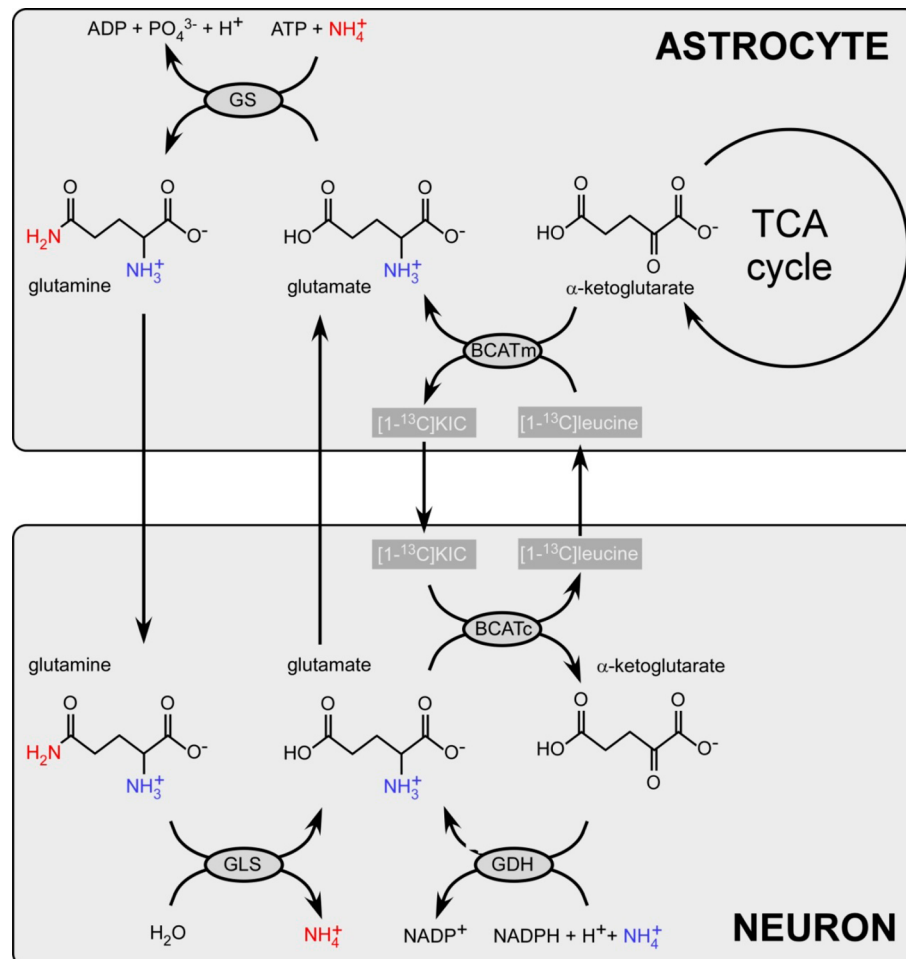


**Figure 14.** Schematic representation of the KIC/leucine BCAA cycle along with the coupled glutamine/glutamate cycle active between astrocytes and neurons. To transfer nitrogen from a neuron to an astrocyte, the amino group can be fixed to KIC to form leucine. Abbreviations: GS, glutamine synthetase; BCATm, mitochondrial branched-chain aminotransferase; BCATc, cytosolic branched-chain aminotransferase; GLS, glutaminase; GDH, glutamate dehydrogenase. To effectively move the NH<sub>4</sub><sup>+</sup> from a neuron to an astrocyte, the latter has to be fixed to α-ketoglutarate by mitochondrial GDH.

without wasting expensive labeled material. Finally, besides the obvious necessity for high performance, two prominent practical aspects should also be put forward: the ease of use and the reproducibility. For this reason, we strongly advocate a nearly all automated system, including transfer, infusion/perfusion system, and MR acquisition, similar to what was proposed by Cheng et al.<sup>52</sup> We are confident that the implementation of such a system is technically feasible and that it will soon be developed.

While HP MR has unlocked a new era in *in vivo* imaging with an incredible array of insights into normal and pathophysiology, it has not gained widespread use in traditional areas of (bio)chemical research. There are both scientific and economic concerns that underlie the current state of the field. From the point of view of potential applications of dissolution DNP, metabolomic studies of analytical samples seem like the most clear-cut opportunity for the technology. Progress in this area has been hindered by sample preparation issues. The efficiency of dissolution DNP is highly dependent on the formation of a glass and the uniform distribution of radical in the target sample. It can be challenging to meet these conditions in a sample for a metabolomic study that is composed of hundreds or thousands of compounds. The most typical samples for metabolomic studies have been urine or blood, two biofluids

that are characterized by the presence of high-molecular weight proteins or high salt concentrations. It is the authors' experience that samples with high salt concentrations are difficult to polarize, primarily because of solubility limitations, though there are few discussions of this in the literature. It is most likely that these samples do not glass well, preventing efficient polarization. The presence of simple salts does not prevent extremely high polarizations from being achieved.<sup>178</sup> The Danish company Albeda Research has specialized in the development of substrate preparations for HP <sup>13</sup>C MR.<sup>43,179</sup> Assuming that a proper sample matrix could be identified for a wide range of metabolomic analyses, issues of heterogeneity of nuclear *T*<sub>1</sub> values complicate the interpretation of <sup>13</sup>C spectra that might be collected. Chemical sites with long nuclear *T*<sub>1</sub> values are inherently more sensitive when they are used with dissolution DNP, as opposed to thermally polarized <sup>13</sup>C spectroscopy in which shorter *T*<sub>1</sub> values allow faster repeat times and therefore higher sensitivities. These various factors have combined to make DNP sparsely used at best in metabolomics studies. Another possible field of application could be mechanistic studies in enzymology, where the chemical selectivity of NMR implies that kinetics measurements in isolated systems could be highly informative. Dissolution DNP has already been found to be useful in chemical kinetics,

primarily through the excellent technical work of the Hilty lab.<sup>180–183</sup> However, another experimental detail has prevented the use of DNP for small samples. Both commercially available systems are equipped to solubilize large volumes of sample. The most common dissolution DNP system currently is the HyperSense, which uses a minimum of 3 mL of superheated water to solubilize the frozen sample. Given the sizes of samples regularly produced for enzymology studies, this volume of solvent renders a sample with concentrations too low for study by NMR, or too expensive in terms of sample production. In addition, 3 mL of sample is a volume larger than what can be efficiently used in current systems unless a 10 mm NMR probe is available. Finally, even with rapid delivery systems that have been developed, shimming of the HP sample remains a challenge.<sup>184</sup> From an economic perspective, the HyperSense system costs something more than 600000 USD and the GE SPINLab system is more than 1.5 million USD. This is outside the means of most basic science departments. With all these considerations in mind, development of a dissolution DNP system suitable for use in analytical chemistry should be able to successfully polarize and quantitatively dissolve extremely small samples, preferably using a capillary-based system for sample delivery. A capillary-based NMR system would address concerns about shimming as the sample location does not change relative to the detection coil. The small volumes necessary for capillary NMR systems are ideally suited for analytical applications like metabolomics and enzymology. The primary engineering hurdle that impedes such development is identifying a means for maintaining a small sample at cryogenic temperatures while leaving it subject to dissolution, either by mating a dissolution wand to it or by flushing hot solvent through the containing capillary. Prospects for such a system seem dim unless individual researchers are inclined to take up the development, as biomedical (*in vivo*) applications are driving the field strongly.

## ■ BIOMEDICAL RESEARCH

Given the large number of successful preclinical applications of HP <sup>13</sup>C imaging, it is clear that clinical trials are the next logical step for the technique's development. A trial aimed at establishing safe concentrations of pyruvate for human use was recently completed at UCSF (Figure 15).<sup>55</sup> The ascending dose study found no dose-limiting toxicity even at the maximum dose of 0.43 mL/kg of 230 mM HP [1-<sup>13</sup>C]pyruvate. Comparison to <sup>1</sup>H MRSI methods yielded approximately equivalent SNR levels between the methods, but in at least one case, the lactate/pyruvate ratio identified a previously undiagnosed malignant lesion that was later confirmed as cancerous by biopsy and histopathology. A key point not emphasized in the paper was that because of the extended period needed for the pharmacist to confirm that the sample was suitable for injection (~52 s), a large amount of polarization was lost due to the  $T_1$  of the sample. The new GE SPINLab polarizer has an inline quality control system that will significantly streamline sample production; the take-home message is that in a very real sense the data presented in this paper are the worst we will see from *in vivo* human studies. The quality of the data will only improve.

## ■ THE KILLER APPLICATION?

The acceptance into practice of an imaging modality often hinges on identifying the "killer app", the clinically important

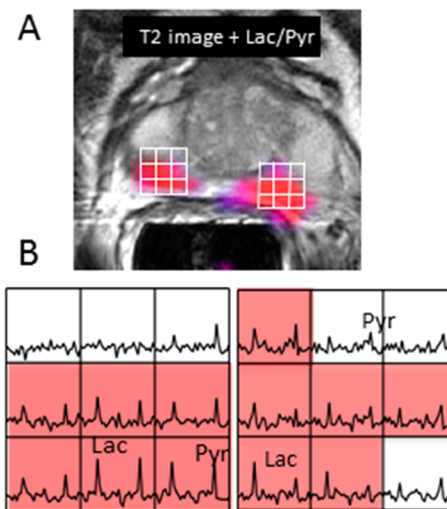


**Figure 15.** Results from the first *in vivo* human experiments using HP [1-<sup>13</sup>C]pyruvate. A CSI sequence identified regions of increased lactate production in prostate cancer that was independently confirmed by biopsy.

problem that can be addressed only with the new technology. Two candidates for HP <sup>13</sup>C imaging have been covered in detail in this review: cancer detection and assessment of healthy and/or damaged cardiac tissue. In the context of cancer in general, prostate cancer may be the most viable clinical target for two reasons. First, while FDG-PET is a very sensitive detector of glucose uptake, prostate cancer is often phenotypically less avid for glucose metabolism than other malignancies. Second, the background signal associated with the bladder can often obscure at least a portion of the prostate. It is no accident that the first use of HP [<sup>13</sup>C]pyruvate in humans was clinically motivated by prostate cancer. Myocardial metabolism seems to be an equally viable target, as the heart consumes such a profligate amount of pyruvate that SNR ratios for imaging experiments can be quite large. The general observation that PDH flux as detected by the production of HP [<sup>13</sup>C]-bicarbonate from [1-<sup>13</sup>C]pyruvate is lower in a variety of models of myocardial pathophysiology should certainly motivate numerous clinical trials once human-use polarizers are fully installed. While this review is hardly all inclusive, it seems clear that HP imaging as a clinical technique will stand or fall on the basis of the success of pyruvate as the agent. With the intellectual and monetary investment already made in HP pyruvate, it is unlikely that other agents, though scientifically important, will have a chance to move forward into clinical practice unless pyruvate is first shown to be a viable agent. Progress with pyruvate as an imaging agent has been considerable. We believe that within a decade "pyruvate scans" for detection of cancer or heart dysfunction (or both) will likely be reimbursed through Medicare.

## ■ AUTHOR INFORMATION

### Corresponding Authors

\*E-mail: arnaud.comment@epfl.ch.

\*E-mail: matthew.merritt@utsouthwestern.edu.

### Funding

M.E.M. is supported by funding through National Institutes of Health Grants P41 EB015908, R21 EB016197, R37 HL34557, and CPRIT RP-101243. A.C. is supported by the Swiss National Science Foundation (Grant PP00P2\_133562) and the

Centre d'Imagerie BioMédicale (CIBM) of the UNIL, UNIGE, HUG, CHUV, EPFL, and the Leenards and Jeantet Foundations.

### Notes

The authors declare no competing financial interest.

### ACKNOWLEDGMENTS

We thank Dr. Hikari Ananda Infinity Yoshihara for his suggestions and for proofreading the manuscript and Emine Can for preparing Figure 4.

### ABBREVIATIONS

MR, magnetic resonance; MRI, magnetic resonance imaging; MRS, magnetic resonance spectroscopy; HP, hyperpolarized; DNP, dynamic nuclear polarization; PHIP, parahydrogen-induced polarization; NMR, nuclear magnetic resonance; MAS, magic-angle spinning; pO<sub>2</sub>, oxygen partial pressure; FDG, 2-deoxy-2-[<sup>18</sup>F]fluoroglucose; PET, positron emission tomography; NAD, nicotinamide adenine dinucleotide; SNR, signal-to-noise ratio; CSI, chemical shift imaging; LDH, lactate dehydrogenase; UCSF, University of California San Francisco; TRAMP, transgenic adenocarcinoma model of mouse prostate; EPSI, echo planar spectroscopic imaging; THC, total hyperpolarized carbon; MCT, monocarboxylate transporter; DCA, dichloroacetic acid; ATC, anaplastic thyroid cancer; 2-DG, 2-deoxyglucose; ROS, reactive oxygen species; DCE, dynamic contrast enhanced; CoA, coenzyme A; TCA, tricarboxylic acid; ALT, alanine aminotransferase; PDH, pyruvate dehydrogenase; PK, pyruvate kinase; PC, pyruvate carboxylase; HF, heart failure; PEPCK, phosphoenolpyruvate carboxykinase; KO, knockout; k<sub>app</sub>, apparent rate constant; POCE, proton-observed carbon-edited; LCFA, long-chain fatty acid; Asc, ascorbate; DHA, dehydroascorbate; GLUT, glucose transporter; DKG, diketogulonate; LD, lethal dosage; GSH, glutathione; GSSH, glutathione disulfide; GR, glutathione reductase; DHAR, dehydroascorbate reductase; α-KG, α-ketoglutarate; GLS, glutaminase; ATR, aminotransferase; GDH, glutamate dehydrogenase; HIF, hypoxia-inducible factor; IDH, isocitrate dehydrogenase; KIC, α-ketoisocaproate; BCKA, α-keto acid; BCAA, branched-chain amino acid; BCAT, branched-chain aminotransferase; CNS, central nervous system; GS, glutamine synthetase; BCATm, mitochondrial branched-chain aminotransferase; BCATc, cytosolic branched-chain aminotransferase.

### REFERENCES

- (1) Gruetter, R., Novotny, E. J., Boulware, S. D., Mason, G. F., Rothman, D. L., Shulman, G. I., Prichard, J. W., and Shulman, R. G. (1994) Localized C-13 Nmr-Spectroscopy in the Human Brain of Amino-Acid Labeling from D-[1-C-13]Glucose. *J. Neurochem.* 63, 1377–1385.
- (2) Gruetter, R., Seaquist, E. R., Kim, S., and Ugurbil, K. (1998) Localized in vivo C-13-NMR of glutamate metabolism in the human brain: Initial results at 4 T. *Dev. Neurosci. (Basel, Switz.)* 20, 380–388.
- (3) Maher, E. A., Marin-Valencia, I., Bachoo, R. M., Mashimo, T., Raisanen, J., Hatapaa, K. J., Jindal, A., Jeffrey, F. M., Choi, C. H., Madden, C., Mathews, D., Pascual, J. M., Mickey, B. E., Malloy, C. R., and DeBerardinis, R. J. (2012) Metabolism of [U-<sup>13</sup>C]glucose in human brain tumors in vivo. *NMR Biomed.* 25, 1234–1244.
- (4) Shulman, R. G., and Rothman, D. L. (2001) <sup>13</sup>C NMR of intermediary metabolism: Implications for systemic physiology. *Annu. Rev. Physiol.* 63, 15–48.
- (5) van de Ven, K. C. C., de Galan, B. E., van der Graaf, M., Shestov, A. A., Henry, P. G., Tack, C. J. J., and Heerschap, A. (2011) Effect of Acute Hypoglycemia on Human Cerebral Glucose Metabolism Measured by C-13 Magnetic Resonance Spectroscopy. *Diabetes* 60, 1467–1473.
- (6) Duarte, J. M., Lanz, B., and Gruetter, R. (2011) Compartmentalized Cerebral Metabolism of [1,6-C]Glucose Determined by in vivo C NMR Spectroscopy at 14.1 T. *Front. Neuroenerg.* 3, 3.
- (7) Henry, P. G., Adriany, G., Deelchand, D., Gruetter, R., Marjanska, M., Oz, G., Seaquist, E. R., Shestov, A., and Ugurbil, K. (2006) In vivo C-13 NMR spectroscopy and metabolic modeling in the brain: A practical perspective. *Magn. Reson. Imaging* 24, 527–539.
- (8) Lanz, B., Gruetter, R., and Duarte, J. M. (2013) Metabolic Flux and Compartmentation Analysis in the Brain In vivo. *Front. Endocrinol.* 4, 156.
- (9) Sherry, A. D., and Malloy, C. R. (2002) <sup>13</sup>C Isotopomer Analysis of Glutamate: A NMR Method to Probe Metabolic Pathways Intersecting in the Citric Acid Cycle. In *In Vivo Carbon-13 NMR* (Berliner, L. J., and Robitaille, P.-M., Eds.) pp 59–97, Kluwer Academic Publishers, Dordrecht, The Netherlands.
- (10) Comment, A. (2013) CHAPTER 9 Hyperpolarization: Concepts, Techniques and Applications. In *New Applications of NMR in Drug Discovery and Development*, pp 252–272, The Royal Society of Chemistry, Cambridge, U.K.
- (11) Overhauser, A. W. (1953) Polarization of Nuclei in Metals. *Phys. Rev.* 92, 411–415.
- (12) Carver, T. R., and Slichter, C. P. (1953) Polarization of Nuclear Spins in Metals. *Phys. Rev.* 92, 212–213.
- (13) Abragam, A., and Goldman, M. (1982) *Nuclear Magnetism: Order and Disorder*, Oxford University Press, Oxford, U.K.
- (14) Becerra, L. R., Gerfen, G. J., Temkin, R. J., Singel, D. J., and Griffin, R. G. (1993) Dynamic Nuclear-Polarization with a Cyclotron-Resonance Maser at 5-T. *Phys. Rev. Lett.* 71, 3561–3564.
- (15) Golman, K., Leunbach, I., Petersson, J. S., Holz, D., and Overweg, J. (2002) Overhauser-enhanced MRI. *Academic Radiology* 9, S104–S108.
- (16) Ardenkjær-Larsen, J. H., Fridlund, B., Gram, A., Hansson, G., Hansson, L., Lerche, M. H., Servin, R., Thaning, M., and Golman, K. (2003) Increase in signal-to-noise ratio of > 10,000 times in liquid-state NMR. *Proc. Natl. Acad. Sci. U.S.A.* 100, 10158–10163.
- (17) Comment, A., van den Brandt, B., Uffmann, K., Kurdzesau, F., Jannin, S., Konter, J. A., Hautle, P., Wenckebach, W. T., Gruetter, R., and van der Klink, J. J. (2007) Design and performance of a DNP prepolarizer coupled to a rodent MRI scanner. *Concepts Magn. Reson., Part B* 31B, 255–269.
- (18) Eichhorn, T. R., Haag, M., van den Brandt, B., Hautle, P., Wenckebach, W. T., Jannin, S., van der Klink, J. J., and Comment, A. (2013) An apparatus for pulsed ESR and DNP experiments using optically excited triplet states down to liquid helium temperatures. *J. Magn. Reson.* 234, 58–66.
- (19) Eichhorn, T. R., Takado, Y., Salameh, N., Capozzi, A., Cheng, T., Hyacinthe, J. N., Mishkovsky, M., Roussel, C., and Comment, A. (2013) Hyperpolarization without persistent radicals for in vivo real-time metabolic imaging. *Proc. Natl. Acad. Sci. U.S.A.* 110, 18064–18069.
- (20) Goertz, S. T., Harmsen, J., Heckmann, J., Hess, C., Meyer, W., Radtke, E., and Reicherz, G. (2004) Highest polarizations in deuterated compounds. *Nucl. Instrum. Methods Phys. Res., Sect. A* 526, 43–52.
- (21) Wolber, J., Ellner, F., Fridlund, B., Gram, A., Johannesson, H., Hansson, G., Hansson, L. H., Lerche, M. H., Mansson, S., Servin, R., Thaning, M., Golman, K., and Ardenkjær-Larsen, J. H. (2004) Generating highly polarized nuclear spins in solution using dynamic nuclear polarization. *Nucl. Instrum. Methods Phys. Res., Sect. A* 526, 173–181.
- (22) Krahn, A., Lottmann, P., Marquardsen, T., Tavernier, A., Turke, M. T., Reese, M., Leonov, A., Bennati, M., Hoefer, P., Engelke, F., and Griesinger, C. (2010) Shuttle DNP spectrometer with a two-center magnet. *Phys. Chem. Chem. Phys.* 12, 5830–5840.
- (23) Krummenacker, J. G., Denysenkov, V. P., Terekhov, M., Schreiber, L. M., and Prisner, T. F. (2012) DNP in MRI: An in-bore approach at 1.5 T. *J. Magn. Reson.* 215, 94–99.

- (24) Lingwood, M. D., Siaw, T. A., Sailsuta, N., Ross, B. D., Bhattacharya, P., and Han, S. G. (2010) Continuous flow Overhauser dynamic nuclear polarization of water in the fringe field of a clinical magnetic resonance imaging system for authentic image contrast. *J. Magn. Reson.* **205**, 247–254.
- (25) Kveder, M., Merunka, D., Jokic, M., Makarevic, J., and Rakvin, B. (2009) Electron spin-lattice relaxation in solid ethanol: Effect of nitroxyl radical hydrogen bonding and matrix disorder. *Phys. Rev. B* **80**, 052201.
- (26) Lumata, L., Kovacs, Z., Sherry, A. D., Malloy, C., Hill, S., van Tol, J., Yu, L., Song, L., and Merritt, M. E. (2013) Electron spin resonance studies of trityl OX063 at a concentration optimal for DNP. *Phys. Chem. Chem. Phys.* **15**, 9800–9807.
- (27) Jannin, S., Comment, A., Kurdzesau, F., Konter, J. A., Hautle, P., van den Brandt, B., and van der Klink, J. J. (2008) A 140 GHz prepolarizer for dissolution dynamic nuclear polarization. *J. Chem. Phys.* **128**, 241102.
- (28) Johannesson, H., Macholl, S., and Ardenkjaer-Larsen, J. H. (2009) Dynamic Nuclear Polarization of [ $^{13}\text{C}$ ]pyruvic acid at 4.6 T. *J. Magn. Reson.* **197**, 167–175.
- (29) Cheng, T., Capozzi, A., Takado, Y., Balzan, R., and Comment, A. (2013) Over 35% liquid-state C-13 polarization obtained via dissolution dynamic nuclear polarization at 7 T and 1 K using ubiquitous nitroxyl radicals. *Phys. Chem. Chem. Phys.* **15**, 20819–20822.
- (30) Armstrong, B. D., Edwards, D. T., Wylde, R. J., Walker, S. A., and Han, S. I. (2010) A 200 GHz dynamic nuclear polarization spectrometer. *Phys. Chem. Chem. Phys.* **12**, 5920–5926.
- (31) Jannin, S., Comment, A., and van der Klink, J. J. (2012) Dynamic Nuclear Polarization by Thermal Mixing Under Partial Saturation. *Appl. Magn. Reson.* **43**, 59–68.
- (32) Comment, A., Rentsch, J., Kurdzesau, F., Jannin, S., Uffmann, K., van Heeswijk, R. B., Hautle, P., Konter, J. A., van den Brandt, B., and van der Klink, J. J. (2008) Producing over 100 mL of highly concentrated hyperpolarized solution by means of dissolution DNP. *J. Magn. Reson.* **194**, 152–155.
- (33) Comment, A., van den Brandt, B., Uffmann, K., Kurdzesau, F., Jannin, S., Konter, J. A., Hautle, P., Wenckebach, W. T., Gruetter, R., and van der Klink, J. J. (2008) Principles of operation of a DNP prepolarizer coupled to a rodent MRI scanner. *Appl. Magn. Reson.* **34**, 313–319.
- (34) Lumata, L., Martin, R., Jindal, A., Kovacs, Z., Conradi, M., and Merritt, M. (2014) Development and performance of a 129-GHz dynamic nuclear polarizer in an ultra-wide bore superconducting magnet. *Magn. Reson. Mater. Phys., Biol. Med.*, 1–11.
- (35) Lumata, L., Ratnakar, S. J., Jindal, A., Merritt, M., Comment, A., Malloy, C., Sherry, A. D., and Kovacs, Z. (2011) BDPA: An Efficient Polarizing Agent for Fast Dissolution Dynamic Nuclear Polarization NMR Spectroscopy. *Chemistry* **17**, 10825–10827.
- (36) Kurdzesau, F., van den Brandt, B., Comment, A., Hautle, P., Jannin, S., van der Klink, J. J., and Konter, J. A. (2008) Dynamic nuclear polarization of small labelled molecules in frozen water-alcohol solutions. *J. Phys. D: Appl. Phys.* **41**, 155506.
- (37) Bornet, A., Melzi, R., Linde, A. J. P., Hautle, P., van den Brandt, B., Jannin, S., and Bodenhausen, G. (2013) Boosting Dissolution Dynamic Nuclear Polarization by Cross Polarization. *J. Phys. Chem. Lett.* **4**, 111–114.
- (38) Lumata, L., Merritt, M. E., and Kovacs, Z. (2013) Influence of deuteration in the glassing matrix on  $^{13}\text{C}$  dynamic nuclear polarization. *Phys. Chem. Chem. Phys.* **15**, 7032–7035.
- (39) Bastiaansen, J. A. M.; Merritt, M. E.; Comment, A. Measuring In Vivo Myocardial Substrate Preference in Real Time Using Hyperpolarized  $^{13}\text{C}$  Magnetic Resonance. In *Proceedings of the International Society for Magnetic Resonance in Medicine*, 2014, Vol. 22, Milan.
- (40) Comment, A. (2014) The benefits of not using exogenous substances to prepare substrates for hyperpolarized MRI. *Imaging Med.* **6**, 1–3.
- (41) Ardenkjaer-Larsen, J. H., Macholl, S., and Johannesson, H. (2008) Dynamic nuclear polarization with trityls at 1.2 K. *Appl. Magn. Reson.* **34**, 509–522.
- (42) Lumata, L., Merritt, M. E., Malloy, C. R., Sherry, A. D., and Kovacs, Z. (2012) Impact of  $\text{Gd}^{3+}$  on DNP of [ $^{13}\text{C}$ ]Pyruvate Doped with Trityl OX063, BDPA, or 4-Oxo-TEMPO. *J. Phys. Chem. A* **116**, 5129–5138.
- (43) Karlsson, M., Jensen, P. R., Duus, J. O., Meier, S., and Lerche, M. H. (2012) Development of Dissolution DNP-MR Substrates for Metabolic Research. *Appl. Magn. Reson.* **43**, 223–236.
- (44) Cudalbu, C., Comment, A., Kurdzesau, F., van Heeswijk, R. B., Uffmann, K., Jannin, S., Denisov, V., Kirik, D., and Gruetter, R. (2010) Feasibility of in vivo N-15 MRS detection of hyperpolarized N-15 labeled choline in rats. *Phys. Chem. Chem. Phys.* **12**, 5818–5823.
- (45) Gabellieri, C., Reynolds, S., Lavie, A., Payne, G. S., Leach, M. O., and Ekyun, T. R. (2008) Therapeutic target metabolism observed using hyperpolarized N-15 choline. *J. Am. Chem. Soc.* **130**, 4598–4599.
- (46) Gallagher, F. A., Kettunen, M. I., and Brindle, K. M. (2009) Biomedical applications of hyperpolarized C-13 magnetic resonance imaging. *Prog. Nucl. Magn. Reson. Spectrosc.* **55**, 285–295.
- (47) Lumata, L., Merritt, M. E., Hashami, Z., Ratnakar, S. J., and Kovacs, Z. (2012) Production and NMR characterization of hyperpolarized (107,109) ag complexes. *Angew. Chem., Int. Ed.* **51**, 525–527.
- (48) Merritt, M. E., Mishkovsky, M., Cheng, T., Jindal, A., Kovacs, Z., Malloy, C. R., Gruetter, R., Sherry, A. D., and Comment, A. (2010) In vivo hyperpolarized  $^{89}\text{Y}$  studies in a 9.4T animal scanner. In *Proceedings of the International Society of Magnetic Resonance in Medicine*, Vol. 18, Stockholm.
- (49) Mishkovsky, M., and Frydman, L. (2008) Progress in hyperpolarized ultrafast 2D NMR spectroscopy. *ChemPhysChem* **9**, 2340–2348.
- (50) Sarkar, R., Comment, A., Vasos, P. R., Jannin, S., Gruetter, R., Bodenhausen, G., Hall, H., Kirik, D., and Denisov, V. P. (2009) Proton NMR of N-15-Choline Metabolites Enhanced by Dynamic Nuclear Polarization. *J. Am. Chem. Soc.* **131**, 16014–16015.
- (51) van Heeswijk, R. B., Uffmann, K., Comment, A., Kurdzesau, F., Perazzolo, C., Cudalbu, C., Jannin, S., Konter, J. A., Hautle, P., van den Brandt, B., Navon, G., van der Klink, J. J., and Gruetter, R. (2009) Hyperpolarized Lithium-6 as a Sensor of Nanomolar Contrast Agents. *Magn. Reson. Med.* **61**, 1489–1493.
- (52) Cheng, T., Mishkovsky, M., Bastiaansen, J. A. M., Ouari, O., Hautle, P., Tordo, P., van den Brandt, B., and Comment, A. (2013) Automated transfer and injection of hyperpolarized molecules with polarization measurement prior to in vivo NMR. *NMR Biomed.* **26**, 1582–1588.
- (53) Mieville, P., Ahuja, P., Sarkar, R., Jannin, S., Vasos, P. R., Gerber-Lemaire, S., Mishkovsky, M., Comment, A., Gruetter, R., Ouari, O., Tordo, P., and Bodenhausen, G. (2010) Scavenging Free Radicals To Preserve Enhancement and Extend Relaxation Times in NMR using Dynamic Nuclear Polarization. *Angew. Chem., Int. Ed.* **49**, 6182–6185.
- (54) Ardenkjaer-Larsen, J. H., Leach, A. M., Clarke, N., Urbahn, J., Anderson, D., and Skloss, T. W. (2011) Dynamic Nuclear Polarization Polarizer for Sterile Use Intent. *NMR Biomed.* **24**, 927–932.
- (55) Nelson, S. J., Kurhanewicz, J., Vigneron, D. B., Larson, P. E., Harzstark, A. L., Ferrone, M., van Criekinge, M., Chang, J. W., Bok, R., Park, I., Reed, G., Carvajal, L., Small, E. J., Munster, P., Weinberg, V. K., Ardenkjaer-Larsen, J. H., Chen, A. P., Hurd, R. E., Odegardstuen, L. I., Robb, F. J., Tropp, J., and Murray, J. A. (2013) Metabolic Imaging of Patients with Prostate Cancer Using Hyperpolarized [ $^{13}\text{C}$ ]Pyruvate. *Sci. Transl. Med.* **5**, 198ra108.
- (56) Vasos, P. R., Comment, A., Sarkar, R., Ahuja, P., Jannin, S., Ansermet, J. P., Konter, J. A., Hautle, P., van den Brandt, B., and Bodenhausen, G. (2009) Long-lived states to sustain hyperpolarized magnetization. *Proc. Natl. Acad. Sci. U.S.A.* **106**, 18469–18473.
- (57) Warren, W. S., Jenista, E., Branca, R. T., and Chen, X. (2009) Increasing Hyperpolarized Spin Lifetimes Through True Singlet Eigenstates. *Science* **323**, 1711–1714.

- (58) Larson, P. E. Z., Kerr, A. B., Chen, A. P., Lustig, M. S., Zierhut, M. L., Hu, S., Cunningham, C. H., Pauly, J. M., Kurhanewicz, J., and Vigneron, D. B. (2008) Multiband excitation pulses for hyperpolarized C-13 dynamic chemical-shift imaging. *J. Magn. Reson.* 194, 121–127.
- (59) Lau, A. Z., Chen, A. P., Hurd, R. E., and Cunningham, C. H. (2011) Spectral-spatial excitation for rapid imaging of DNP compounds. *NMR Biomed.* 24, 988–996.
- (60) Leupold, J., Mansson, S., Petersson, J. S., Hennig, J., and Wieben, O. (2009) Fast multiecho balanced SSFP metabolite mapping of <sup>1</sup>H and hyperpolarized <sup>13</sup>C compounds. *MAGMA* 22, 251–256.
- (61) von Morze, C., Reed, G., Shin, P., Larson, P. E. Z., Hu, S., Bok, R., and Vigneron, D. B. (2011) Multi-band frequency encoding method for metabolic imaging with hyperpolarized [1-C-13]pyruvate. *J. Magn. Reson.* 211, 109–113.
- (62) Chekmenev, E. Y., Norton, V. A., Weitekamp, D. P., and Bhattacharya, P. (2009) Hyperpolarized H-1 NMR Employing Low gamma Nucleus for Spin Polarization Storage. *J. Am. Chem. Soc.* 131, 3164–3165.
- (63) Mishkovsky, M., Cheng, T., Comment, A., and Gruetter, R. (2012) Localized *in vivo* hyperpolarization transfer sequences. *Magn. Reson. Med.* 68, 349–352.
- (64) Mishkovsky, M., Comment, A., and Gruetter, R. (2012) *In vivo* detection of brain Krebs cycle intermediate by hyperpolarized magnetic resonance. *J. Cereb. Blood Flow Metab.* 32, 2108–2113.
- (65) Keshari, K. R., and Wilson, D. M. (2014) Chemistry and biochemistry of <sup>13</sup>C hyperpolarized magnetic resonance using dynamic nuclear polarization. *Chem. Soc. Rev.* 43, 1627–1659.
- (66) Zhang, H. (2014) The Potential of Hyperpolarized <sup>13</sup>C MRI in Assessing Signaling Pathways in Cancer. *Academic Radiology* 21, 215–222.
- (67) Krishna, M. C., Matsumoto, S., Saito, K., Matsuo, M., Mitchell, J. B., and Ardenkjær-Larsen, J. H. (2013) Magnetic resonance imaging of tumor oxygenation and metabolic profile. *Acta Oncol.* 52, 1248–1256.
- (68) Tyler, D. J. (2011) Cardiovascular Applications of Hyperpolarized MRI. *Current Cardiovascular Imaging Reports* 4, 108–115.
- (69) Pilkis, S. J., and Granner, D. K. (1992) Molecular Physiology of the Regulation of Hepatic Gluconeogenesis and Glycolysis. *Annu. Rev. Physiol.* 54, 885–909.
- (70) Warburg, O. (1956) On the origin of cancer cells. *Science* 123, 309–314.
- (71) Kurhanewicz, J., Vigneron, D. B., Brindle, K., Chekmenev, E. Y., Comment, A., Cunningham, C. H., Deberardinis, R. J., Green, G. G., Leach, M. O., Rajan, S. S., Rizi, R. R., Ross, B. D., Warren, W. S., and Malloy, C. R. (2011) Analysis of cancer metabolism by imaging hyperpolarized nuclei: Prospects for translation to clinical research. *Neoplasia* 13, 81–97.
- (72) Meier, S., Karlsson, M., Jensen, P. R., Lerche, M. H., and Duus, J. Ø. (2011) Metabolic pathway visualization in living yeast by DNP-NMR. *Mol. BioSyst.* 7, 2834–2836.
- (73) Harris, T., Degani, H., and Frydman, L. (2013) Hyperpolarized <sup>13</sup>C NMR studies of glucose metabolism in living breast cancer cell cultures. *NMR Biomed.* 26, 1831–1843.
- (74) Allouche-Aron, H., Wade, T., Waldner, L. F., Miller, V. N., Gomori, J. M., Katz-Bull, R., and McKenzie, C. A. (2013) *In vivo* magnetic resonance imaging of glucose: Initial experience. *Contrast Media Mol. Imaging* 8, 72–82.
- (75) Rodrigues, T. B., Serrao, E. M., Kennedy, B. W., Hu, D. E., Kettunen, M. I., and Brindle, K. M. (2014) Magnetic resonance imaging of tumor glycolysis using hyperpolarized C-labeled glucose. *Nat. Med.* 20, 93–97.
- (76) Christensen, C. E., Karlsson, M., Winther, J. R., Jensen, P. R., and Lerche, M. H. (2014) Non-invasive In-cell Determination of Free Cytosolic [NAD<sup>+</sup>]/[NADH] Ratios Using Hyperpolarized Glucose Show Large Variations in Metabolic Phenotypes. *J. Biol. Chem.* 289, 2344–2352.
- (77) Williamson, D. H., Lund, P., and Krebs, H. A. (1967) The redox state of free nicotinamide-adenine dinucleotide in the cytoplasm and mitochondria of rat liver. *Biochem. J.* 103, 514–527.
- (78) Golman, K., In't Zandt, R., Lerche, M. H., Pehrson, R., and Ardenkjær-Larsen, J. H. (2006) Metabolic imaging by hyperpolarized <sup>13</sup>C magnetic resonance imaging for *in vivo* tumor diagnosis. *Cancer Res.* 66, 10855–10860.
- (79) Day, S. E., Kettunen, M. I., Gallagher, F. A., De-En, H., Lerche, M., Wolber, J., Golman, K., Ardenkjær-Larsen, J. H., and Brindle, K. M. (2007) Detecting tumor response to treatment using hyperpolarized <sup>13</sup>C magnetic resonance imaging and spectroscopy. *Nat. Med.* 13, 1382–1387.
- (80) Chen, A. P., Albers, M. J., Cunningham, C. H., Kohler, S. J., Yen, Y. F., Hurd, R. E., Tropp, J., Bok, R., Pauly, J. M., Nelson, S. J., Kurhanewicz, J., and Vigneron, D. B. (2007) Hyperpolarized C-13 spectroscopic imaging of the TRAMP mouse at 3T-initial experience. *Magn. Reson. Med.* 58, 1099–1106.
- (81) Chen, A. P., Cunningham, C. H., Ozturk-Isik, E., Xu, D., Hurd, R. E., Kelley, D. A., Pauly, J. M., Kurhanewicz, J., Nelson, S. J., and Vigneron, D. B. (2007) High-speed 3T MR spectroscopic imaging of prostate with flyback echo-planar encoding. *J. Magn. Reson. Imaging* 25, 1288–1292.
- (82) Albers, M. J., Bok, R., Chen, A. P., Cunningham, C. H., Zierhut, M. L., Zhang, V. Y., Kohler, S. J., Tropp, J., Hurd, R. E., Yen, Y. F., Nelson, S. J., Vigneron, D. B., and Kurhanewicz, J. (2008) Hyperpolarized <sup>13</sup>C lactate, pyruvate, and alanine: Noninvasive biomarkers for prostate cancer detection and grading. *Cancer Res.* 68, 8607–8615.
- (83) Park, I., Larson, P. E., Zierhut, M. L., Hu, S., Bok, R., Ozawa, T., Kurhanewicz, J., Vigneron, D. B., Vandenberg, S. R., James, C. D., and Nelson, S. J. (2010) Hyperpolarized <sup>13</sup>C magnetic resonance metabolic imaging: Application to brain tumors. *Neuro-Oncology* (Cary, NC, U.S.) 12, 133–144.
- (84) Ward, C. S., Venkatesh, H. S., Chaumeil, M. M., Brandes, A. H., VanCrieke, M., Dafni, H., Sukumar, S., Nelson, S. J., Vigneron, D. B., Kurhanewicz, J., James, C. D., Haas-Kogan, D. A., and Ronen, S. M. (2010) Noninvasive Detection of Target Modulation following Phosphatidylinositol 3-Kinase Inhibition Using Hyperpolarized <sup>13</sup>C Magnetic Resonance Spectroscopy. *Cancer Res.* 70, 1296–1305.
- (85) Dafni, H., Larson, P. E., Hu, S., Yoshihara, H. A., Ward, C. S., Venkatesh, H. S., Wang, C., Zhang, X., Vigneron, D. B., and Ronen, S. M. (2010) Hyperpolarized <sup>13</sup>C spectroscopic imaging informs on hypoxia-inducible factor-1 and myc activity downstream of platelet-derived growth factor receptor. *Cancer Res.* 70, 7400–7410.
- (86) Senadheera, L., Mayer, D., Josan, S., Darpolar, M., Luong, R., Yen, Y., Spielman, D., and Xing, L. (2011) TU-A-BRC-02: Hyperpolarized <sup>13</sup>C MRSI for Assessing Radiation Response of Prostate Cancer in Transgenic Mice. *Med. Phys.* 38, 3741–3742.
- (87) Seth, P., Grant, A., Tang, J., Vinogradov, E., Wang, X., Lenkinski, R., and Sukhatme, V. P. (2011) On-target inhibition of tumor fermentative glycolysis as visualized by hyperpolarized pyruvate. *Neoplasia* 13, 60–71.
- (88) Sandulache, V. C., Skinner, H. D., Wang, Y., Chen, Y., Dodge, C. T., Ow, T. J., Bankson, J. A., Myers, J. N., and Lai, S. Y. (2012) Glycolytic Inhibition Alters Anaplastic Thyroid Carcinoma Tumor Metabolism and Improves Response to Conventional Chemotherapy and Radiation. *Mol. Cancer Ther.* 11, 1373–1380.
- (89) Sandulache, V. C., Chen, Y., Lee, J., Rubinstein, A., Ramirez, M. S., Skinner, H. D., Walker, C. M., Williams, M. D., Tailor, R., Court, L. E., Bankson, J. A., and Lai, S. Y. (2014) Evaluation of hyperpolarized [1-<sup>13</sup>C]-pyruvate by magnetic resonance to detect ionizing radiation effects in real time. *PLoS One* 9, e87031.
- (90) Bohndiek, S. E., Kettunen, M. I., Hu, D.-e., and Brindle, K. M. (2012) Hyperpolarized <sup>13</sup>C Spectroscopy Detects Early Changes in Tumor Vasculature and Metabolism after VEGF Neutralization. *Cancer Res.* 72, 854–864.
- (91) Gallagher, F. A., Kettunen, M. I., Hu, D. E., Jensen, P. R., Zandt, R. I., Karlsson, M., Gisselsson, A., Nelson, S. K., Witney, T. H., Bohndiek, S. E., Hansson, G., Peitersen, T., Lerche, M. H., and Brindle, K. M. (2009) Production of hyperpolarized [1,4-<sup>13</sup>C<sub>2</sub>]malate from [1,4-<sup>13</sup>C<sub>2</sub>]fumarate is a marker of cell necrosis and treatment response in tumors. *Proc. Natl. Acad. Sci. U.S.A.* 106, 19801–19806.

- (92) Dutta, P., Le, A., Vander Jagt, D. L., Tsukamoto, T., Martinez, G. V., Dang, C. V., and Gillies, R. J. (2013) Evaluation of LDH-A and Glutaminase Inhibition In Vivo by Hyperpolarized  $^{13}\text{C}$ -Pyruvate Magnetic Resonance Spectroscopy of Tumors. *Cancer Res.* 73, 4190–4195.
- (93) Lodi, A., Woods, S. M., and Ronen, S. M. (2013) Treatment with the MEK inhibitor U0126 induces decreased hyperpolarized pyruvate to lactate conversion in breast, but not prostate, cancer cells. *NMR Biomed.* 26, 299–306.
- (94) Asghar Butt, S., Søgaard, L. V., Ardenkjaer-Larsen, J. H., Lauritzen, M. H., Engelholm, L. H., Paulson, O. B., Mirza, O., Holck, S., Magnusson, P., and Åkeson, P. (2014) Monitoring mammary tumor progression and effect of tamoxifen treatment in MMTV-PymT using MRI and magnetic resonance spectroscopy with hyperpolarized [ $1\text{-}^{13}\text{C}$ ]pyruvate. *Magn. Reson. Med.*, DOI: 10.1002/mrm.25095.
- (95) Xu, H. N., Kadlecak, S., Profka, H., Glickson, J. D., Rizi, R., and Li, L. Z. (2014) Is Higher Lactate an Indicator of Tumor Metastatic Risk? A Pilot MRS Study Using Hyperpolarized  $^{13}\text{C}$ -Pyruvate. *Academic Radiology* 21, 223–231.
- (96) Thind, K., Jensen, M. D., Hegarty, E., Chen, A. P., Lim, H., Martinez-Santiesteban, F., Van Dyk, J., Wong, E., Scholl, T. J., and Santyr, G. E. (2014) Mapping metabolic changes associated with early radiation induced lung injury post conformal radiotherapy using hyperpolarized  $^{13}\text{C}$ -pyruvate magnetic resonance spectroscopic imaging. *Radiother. Oncol.* 110, 317–322.
- (97) MacKenzie, J. D., Yen, Y. F., Mayer, D., Tropp, J. S., Hurd, R. E., and Spielman, D. M. (2011) Detection of Inflammatory Arthritis by Using Hyperpolarized C-13-Pyruvate with MR Imaging and Spectroscopy. *Radiology* 259, 414–420.
- (98) Witney, T. H., Kettunen, M. I., Day, S. E., Hu, D.-E., Neves, A. A., Gallagher, F. A., Fulton, S. M., and Brindle, K. M. (2009) A Comparison between Radiolabeled Fluorodeoxyglucose Uptake and Hyperpolarized  $^{13}\text{C}$ -Labeled Pyruvate Utilization as Methods for Detecting Tumor Response to Treatment. *Neoplasia* 11, 574–582.
- (99) Weidl, E., Menzel, M., Janich, M., Khegai, O., Wiesinger, F., Haase, A., Nekolla, S., Schulte, R., and Schwaiger, M. (2012) In vivo detection of tumor metabolism with  $^{18}\text{F}$ -FDG PET and hyperpolarized [ $1\text{-}^{13}\text{C}$ ]-pyruvate magnetic resonance spectroscopic imaging. *Journal of Nuclear Medicine Meeting Abstracts* 53, 516.
- (100) Holmes, F. L. (1980) Hans Krebs and the discovery of the ornithine cycle. *Fed. Proc.* 216.
- (101) Atherton, H. J., Schroeder, M. A., Dodd, M. S., Heather, L. C., Carter, E. E., Cochlin, L. E., Nagel, S., Sibson, N. R., Radda, G. K., Clarke, K., and Tyler, D. J. (2011) Validation of the in vivo assessment of pyruvate dehydrogenase activity using hyperpolarised  $^{13}\text{C}$  MRS. *NMR Biomed.* 24, 201–208.
- (102) Moreno, K., Sabelhaus, S., Merritt, M., Sherry, A., and Malloy, C. (2009) Effect of Rapid Changes in  $^{13}\text{C}$  Pyruvate Concentration on Lactate and Alanine Pool Sizes and  $^{13}\text{C}$  Enrichment in the Heart. In *Proceedings of the 17th Scientific Meeting, International Society for Magnetic Resonance in Medicine*, Vol. 17, Honolulu, HI.
- (103) Janich, M. A., Menzel, M. I., Wiesinger, F., Weidl, E., Khegai, O., Ardenkjaer-Larsen, J. H., Glaser, S. J., Haase, A., Schulte, R. F., and Schwaiger, M. (2012) Effects of pyruvate dose on in vivo metabolism and quantification of hyperpolarized  $^{13}\text{C}$  spectra. *NMR Biomed.* 25, 142–151.
- (104) Santarelli, M. F., Positano, V., Giovannetti, G., Frijia, F., Menichetti, L., Ardenkjaer-Larsen, J.-H., De Marchi, D., Lionetti, V., Aquaro, G., Lombardi, M., and Landini, L. (2012) How the signal-to-noise ratio influences hyperpolarized  $^{13}\text{C}$  dynamic MRS data fitting and parameter estimation. *NMR Biomed.* 25, 925–934.
- (105) Halestrap, A. P., and Wilson, M. C. (2012) The monocarboxylate transporter family: Role and regulation. *IUBMB Life* 64, 109–119.
- (106) Joseph, S. K., Bradford, N. M., and McGivan, J. D. (1978) Characteristics of the transport of alanine, serine and glutamine across the plasma membrane of isolated rat liver cells. *Biochem. J.* 176, 827–836.
- (107) Jensen, P. R., Karlsson, M., Meier, S., Duus, J. Ø., and Lerche, M. H. (2009) Hyperpolarized Amino Acids for In Vivo Assays of Transaminase Activity. *Chem.—Eur. J.* 15, 10010–10012.
- (108) Bastiaansen, J. M., Yoshihara, H. I., Takado, Y., Gruetter, R., and Comment, A. (2014) Hyperpolarized  $^{13}\text{C}$  lactate as a substrate for in vivo metabolic studies in skeletal muscle. *Metabolomics* 10, 986–994.
- (109) Golman, K., in't Zandt, R., and Thaning, M. (2006) Real Time Metabolic Imaging. *Proc. Natl. Acad. Sci. U.S.A.* 103, 11270–11275.
- (110) Merritt, M. E., Harrison, C., Storey, C., Jeffrey, F. M., Sherry, A. D., and Malloy, C. R. (2007) Hyperpolarized  $^{13}\text{C}$  allows a direct measure of flux through a single enzyme-catalyzed step by NMR. *Proc. Natl. Acad. Sci. U.S.A.* 104, 19773–19777.
- (111) Gallagher, F. A., Kettunen, M. I., Day, S. E., Hu, D.-E., Ardenkjaer-Larsen, J. H., Zandt, R. i. t., Jensen, P. R., Karlsson, M., Golman, K., Lerche, M. H., and Brindle, K. M. (2008) Magnetic resonance imaging of pH in vivo using hyperpolarized  $^{13}\text{C}$ -labelled bicarbonate. *Nature* 453, 940–943.
- (112) Schroeder, M. A., Swietach, P., Atherton, H. J., Gallagher, F. A., Lee, P., Radda, G. K., Clarke, K., and Tyler, D. J. (2010) Measuring intracellular pH in the heart using hyperpolarized carbon dioxide and bicarbonate: A  $^{13}\text{C}$  and  $^{31}\text{P}$  magnetic resonance spectroscopy study. *Cardiovasc. Res.* 86, 82–91.
- (113) Schroeder, M. A., Cochlin, L. E., Heather, L. C., Clarke, K., Radda, G. K., and Tyler, D. J. (2008) In vivo assessment of pyruvate dehydrogenase flux in the heart using hyperpolarized carbon-13 magnetic resonance. *Proc. Natl. Acad. Sci. U.S.A.* 105, 12051–12056.
- (114) Golman, K., Petersson, J. S., Magnusson, P., Johansson, E., Åkeson, P., Chai, C., Hansson, G., and Månnsson, S. (2008) Cardiac metabolism measured noninvasively by hyperpolarized  $^{13}\text{C}$  MRI. *Magn. Reson. Med.* 59, 1005–1013.
- (115) Lau, A. Z., Chen, A. P., Ghugre, N. R., Ramanan, V., Lam, W. W., Connelly, K. A., Wright, G. A., and Cunningham, C. H. (2010) Rapid multislice imaging of hyperpolarized  $^{13}\text{C}$  pyruvate and bicarbonate in the heart. *Magn. Reson. Med.* 64, 1323–1331.
- (116) Schroeder, M. A., Atherton, H. J., Heather, L. C., Griffin, J. L., Clarke, K., Radda, G. K., and Tyler, D. J. (2011) Determining the in vivo regulation of cardiac pyruvate dehydrogenase based on label flux from hyperpolarised [ $1\text{-}^{13}\text{C}$ ]pyruvate. *NMR Biomed.* 24, 980–987.
- (117) Mayer, D., Yen, Y.-F., Josan, S., Park, J. M., Pfefferbaum, A., Hurd, R. E., and Spielman, D. M. (2012) Application of hyperpolarized [ $1\text{-}^{13}\text{C}$ ]lactate for the in vivo investigation of cardiac metabolism. *NMR Biomed.* 25, 1119–1124.
- (118) Merrit, M. E., Harrison, C., Storey, C. J., Sherry, A. D., and Malloy, C. R. (2008) Inhibition of carbohydrate oxidation during the first minute of reperfusion after brief ischemia: NMR detection of hyperpolarized  $^{13}\text{CO}_2$  and  $\text{H}^{13}\text{CO}_3^-$ . *Magn. Reson. Med.* 60, 1029–1036.
- (119) Schroeder, M. A., Atherton, H. J., Ball, D. R., Cole, M. A., Heather, L. C., Griffin, J. L., Clarke, K., Radda, G. K., and Tyler, D. J. (2009) Real-time assessment of Krebs cycle metabolism using hyperpolarized  $^{13}\text{C}$  magnetic resonance spectroscopy. *FASEB J.* 23, 2529–2538.
- (120) Schroeder, M. A., Atherton, H. J., Cochlin, L. E., Clarke, K., Radda, G. K., and Tyler, D. J. (2009) The effect of hyperpolarized tracer concentration on myocardial uptake and metabolism. *Magn. Reson. Med.* 61, 1007–1014.
- (121) Atherton, H. J., Dodd, M. S., Heather, L. C., Schroeder, M. A., Griffin, J. L., Radda, G. K., Clarke, K., and Tyler, D. J. (2011) Role of pyruvate dehydrogenase inhibition in the development of hypertrophy in the hyperthyroid rat heart: a combined magnetic resonance imaging and hyperpolarized magnetic resonance spectroscopy study. *Circulation* 123, 2552–2561.
- (122) Chen, A. P., Hurd, R. E., Schroeder, M. A., Lau, A. Z., Gu, Y. P., Lam, W. W., Barry, J., Tropp, J., and Cunningham, C. H. (2012) Simultaneous investigation of cardiac pyruvate dehydrogenase flux, Krebs cycle metabolism and pH, using hyperpolarized [ $1,2\text{-}^{13}\text{C}_2$ ]-pyruvate in vivo. *NMR Biomed.* 25, 305–311.

- (123) Schroeder, M. A., Lau, A. Z., Chen, A. P., Gu, Y., Nagendran, J., Barry, J., Hu, X., Dyck, J. R. B., Tyler, D. J., Clarke, K., Connelly, K. A., Wright, G. A., and Cunningham, C. H. (2013) Hyperpolarized  $^{13}\text{C}$  magnetic resonance reveals early- and late-onset changes to *in vivo* pyruvate metabolism in the failing heart. *Eur. J. Heart Failure* 15, 130–140.
- (124) Schroeder, M. A., Atherton, H. J., Dodd, M. S., Lee, P., Cochlin, L. E., Radda, G. K., Clarke, K., and Tyler, D. J. (2012) The Cycling of Acetyl-CoA through Acetylcarnitine Buffers Cardiac Substrate Supply: A Hyperpolarised  $^{13}\text{C}$  Magnetic Resonance Study. *Circulation: Cardiovascular Imaging* 5, 201–209.
- (125) Josan, S., Park, J. M., Hurd, R., Yen, Y. F., Pfefferbaum, A., Spielman, D., and Mayer, D. (2013) *In vivo* investigation of cardiac metabolism in the rat using MRS of hyperpolarized [ $1\text{-}^{13}\text{C}$ ] and [ $2\text{-}^{13}\text{C}$ ]pyruvate. *NMR Biomed.* 26, 1680–1687.
- (126) Hu, S., Chen, A. P., Zierhut, M. L., Bok, R., Yen, Y. F., Schroeder, M. A., Hurd, R. E., Nelson, S. J., Kurhanewicz, J., and Vigneron, D. B. (2009) *In vivo* carbon-13 dynamic MRS and MRSI of normal and fasted rat liver with hyperpolarized  $^{13}\text{C}$ -pyruvate. *Molecular Imaging and Biology* 11, 399–407.
- (127) Merritt, M. E., Harrison, C., Sherry, A. D., Malloy, C. R., and Burgess, S. C. (2011) Flux through hepatic pyruvate carboxylase and phosphoenolpyruvate carboxykinase detected by hyperpolarized  $^{13}\text{C}$  magnetic resonance. *Proc. Natl. Acad. Sci. U.S.A.* 108, 19084–19089.
- (128) Lee, P., Leong, W., Tan, T., Lim, M., Han, W., and Radda, G. K. (2013) *In Vivo* hyperpolarized carbon-13 magnetic resonance spectroscopy reveals increased pyruvate carboxylase flux in an insulin-resistant mouse model. *Hepatology* 57, 515–524.
- (129) Moreno, K. X., Jin, E. S., Wang, J.-X., Sherry, A. D., Merritt, M. E., and Malloy, C. R. (2014) Metabolism of Hyperpolarized [ $1\text{-}^{13}\text{C}$ ]Pyruvate to Plasma Glucose in the Rat Liver. In *Proceedings of the International Society of Magnetic Resonance in Medicine*, Vol. 27, May 10–16, Milan.
- (130) Patyal, B. R., Gao, J., Williams, R. F., Roby, J., Saam, B., Rockwell, B. A., Thomas, R. J., Stolarski, D. J., and Fox, P. T. (1997) Longitudinal Relaxation and Diffusion Measurements Using Magnetic Resonance Signals from Laser-Hyperpolarized  $^{129}\text{Xe}$  Nuclei. *J. Magn. Reson.* 126, 58–65.
- (131) Yen, Y. F., Kohler, S. J., Chen, A. P., Tropp, J., Bok, R., Wolber, J., Albers, M. J., Gram, K. A., Zierhut, M. L., Park, I., Zhang, V., Hu, S., Nelson, S. J., Vigneron, D. B., Kurhanewicz, J., Dirven, H. A., and Hurd, R. E. (2009) Imaging considerations for *in vivo*  $^{13}\text{C}$  metabolic mapping using hyperpolarized  $^{13}\text{C}$ -pyruvate. *Magn. Reson. Med.* 62, 1–10.
- (132) Zierhut, M. L., Yen, Y. F., Chen, A. P., Bok, R., Albers, M. J., Zhang, V., Tropp, J., Park, I., Vigneron, D. B., Kurhanewicz, J., Hurd, R. E., and Nelson, S. J. (2009) Kinetic modeling of hyperpolarized  $^{13}\text{C}_1$ -pyruvate metabolism in normal rats and TRAMP mice. *J. Magn. Reson.* 202, 85–92.
- (133) Xu, T., Mayer, D., Gu, M., Yen, Y. F., Josan, S., Tropp, J., Pfefferbaum, A., Hurd, R., and Spielman, D. (2011) Quantification of *in vivo* metabolic kinetics of hyperpolarized pyruvate in rat kidneys using dynamic  $^{13}\text{C}$  MRSI. *NMR Biomed.* 24, 997–1005.
- (134) Harris, T., Eliyahu, G., Frydman, L., and Degan, H. (2009) Kinetics of hyperpolarized  $^{13}\text{C}_1$ -pyruvate transport and metabolism in living human breast cancer cells. *Proc. Natl. Acad. Sci. U.S.A.* 106, 18131–18136.
- (135) Keshari, K. R., Kurhanewicz, J., Jeffries, R. E., Wilson, D. M., Dewar, B. J., Van Criekinge, M., Zierhut, M., Vigneron, D. B., and Macdonald, J. M. (2010) Hyperpolarized  $^{13}\text{C}$  spectroscopy and an NMR-compatible bioreactor system for the investigation of real-time cellular metabolism. *Magn. Reson. Med.* 63, 322–329.
- (136) Witney, T. H., Kettunen, M. I., and Brindle, K. M. (2011) Kinetic modeling of hyperpolarized  $^{13}\text{C}$  label exchange between pyruvate and lactate in tumor cells. *J. Biol. Chem.* 286, 24572–24580.
- (137) Harrison, C., Yang, C., Jindal, A., Deberardinis, R. J., Hooshyar, M. A., Merritt, M., Dean Sherry, A., and Malloy, C. R. (2012) Comparison of kinetic models for analysis of pyruvate-to-lactate exchange by hyperpolarized  $^{13}\text{C}$  NMR. *NMR Biomed.* 25, 1286–1294.
- (138) Yang, C., Harrison, C., Jin, E. S., Chuang, D. T., Sherry, A. D., Malloy, C. R., Merritt, M. E., and Deberardinis, R. J. (2014) Simultaneous Steady-state and Dynamic  $^{13}\text{C}$  NMR Can Differentiate Alternative Routes of Pyruvate Metabolism in Living Cancer Cells. *J. Biol. Chem.* 289, 6212–6224.
- (139) Kettunen, M. I., Hu, D. E., Witney, T. H., McLaughlin, R., Gallagher, F. A., Bohndiek, S. E., Day, S. E., and Brindle, K. M. (2010) Magnetization transfer measurements of exchange between hyperpolarized [ $1\text{-}^{13}\text{C}$ ]pyruvate and [ $1\text{-}^{13}\text{C}$ ]lactate in a murine lymphoma. *Magn. Reson. Med.* 63, 872–880.
- (140) Larson, P. E. Z., Kerr, A. B., Leon Swisher, C., Pauly, J. M., and Vigneron, D. B. (2012) A rapid method for direct detection of metabolic conversion and magnetization exchange with application to hyperpolarized substrates. *J. Magn. Reson.* 225, 71–80.
- (141) Walker, C. M., Lee, J., Ramirez, M. S., Schellingerhout, D., Millward, S., and Bankson, J. A. (2013) A catalyzing phantom for reproducible dynamic conversion of hyperpolarized [ $1\text{-}^{13}\text{C}$ ]-pyruvate. *PLoS One* 8, e71274.
- (142) Fitzpatrick, S. M., Hetherington, H. P., Behar, K. L., and Shulman, R. G. (1990) The Flux from Glucose to Glutamate in the Rat Brain *In Vivo* as Determined by  $^1\text{H}$ -Observed,  $^{13}\text{C}$ -Edited NMR Spectroscopy. *J. Cereb. Blood Flow Metab.* 10, 170–179.
- (143) Ball, D. R., Rowlands, B., Dodd, M. S., Le Page, L., Ball, V., Carr, C. A., Clarke, K., and Tyler, D. J. (2014) Hyperpolarized butyrate: A metabolic probe of short chain fatty acid metabolism in the heart. *Magn. Reson. Med.* 71, 1663–1669.
- (144) Fink, G., Desrochers, S., Des Rosiers, C., Garneau, M., David, F., Dalozze, T., Landau, B. R., and Brunengraber, H. (1988) Pseudoketogenesis in the perfused rat heart. *J. Biol. Chem.* 263, 18036–18042.
- (145) Jensen, P. R., Peitersen, T., Karlsson, M., In't Zandt, R., Gisselsson, A., Hansson, G., Meier, S., and Lerche, M. H. (2009) Tissue-specific short chain fatty acid metabolism and slow metabolic recovery after ischemia from hyperpolarized NMR *in vivo*. *J. Biol. Chem.* 284, 36077–36082.
- (146) Bastiaansen, J. A., Cheng, T., Mishkovsky, M., Duarte, J. M., Comment, A., and Gruetter, R. (2013) *In vivo* enzymatic activity of acetylCoA synthetase in skeletal muscle revealed by  $^{13}\text{C}$  turnover from hyperpolarized [ $1\text{-}^{13}\text{C}$ ]acetate to [ $1\text{-}^{13}\text{C}$ ]acetylcarnitine. *Biochim. Biophys. Acta* 1830, 4171–4178.
- (147) Serra, S. C., Jensen, P. R., Miragoli, L., Karlsson, M., Cabella, C., Poggi, L., Venturi, L., Tedoldi, F., and Lerche, M. (2014) Hyperpolarized [ $1,3\text{-}^{13}\text{C}_2$ ]ethyl acetocacetate is a novel diagnostic marker of liver cancer. In *Proc. Intl. Soc. Mag. Res. in Med.*, Vol. 22, May 10–16, Milan.
- (148) Tyler, D. J., Lau, A. Z., and Ball, D. R. (2014) Hyperpolarized Ketone Body Metabolism in the Perfused Rat Heart. In *Proc. Intl. Soc. Mag. Res. in Med.*, Vol. 22, May 10–16, Milan.
- (149) Brieger, K., Schiavone, S., Miller, F. J., and Krause, K. H. (2012) Reactive oxygen species: From health to disease. *Swiss Med. Wkly.* 142, w13659.
- (150) Deutsch, J. C. (2000) Dehydroascorbic acid. *J. Chromatogr. A* 881, 299–307.
- (151) Deutsch, J. C., and SanthoshKumar, C. R. (1996) Dehydroascorbic acid undergoes hydrolysis on solubilization which can be reversed with mercaptoethanol. *J. Chromatogr. A* 724, 271–278.
- (152) Bohndiek, S. E., Kettunen, M. I., Hu, D. E., Kennedy, B. W. C., Boren, J., Gallagher, F. A., and Brindle, K. M. (2011) Hyperpolarized [ $1\text{-C-13}$ ]-Ascorbic and Dehydroascorbic Acid: Vitamin C as a Probe for Imaging Redox Status in Vivo. *J. Am. Chem. Soc.* 133, 11795–11801.
- (153) Keshari, K. R., Kurhanewicz, J., Bok, R., Larson, P. E. Z., Vigneron, D. B., and Wilson, D. M. (2011) Hyperpolarized C-13 dehydroascorbate as an endogenous redox sensor for *in vivo* metabolic imaging. *Proc. Natl. Acad. Sci. U.S.A.* 108, 18606–18611.
- (154) Patterson, J. W., and Mastin, D. W. (1951) Some Effects of Dehydroascorbic Acid on the Central Nervous System. *Am. J. Physiol.* 167, 119–126.

- (155) Jones, D. P. (2002) Redox potential of GSH/GSSG couple: Assay and biological significance. *Methods Enzymol.* 348, 93–112.
- (156) May, J. M., Mendiratta, S., Hill, K. E., and Burk, R. F. (1997) Reduction of dehydroascorbate to ascorbate by the selenoenzyme thioredoxin reductase. *J. Biol. Chem.* 272, 22607–22610.
- (157) Del Bello, B., Maellaro, E., Sugherini, L., Santucci, A., Comporti, M., and Casini, A. F. (1994) Purification of NADPH-Dependent Dehydroascorbate Reductase from Rat-Liver and Its Identification with 3- $\alpha$ -Hydroxysteroid Dehydrogenase. *Biochem. J.* 304, 385–390.
- (158) Nordberg, J., and Arnér, E. S. J. (2001) Reactive oxygen species, antioxidants, and the mammalian thioredoxin system. *Free Radical Biol. Med.* 31, 1287–1312.
- (159) Wells, W. W., Xu, D. P., Yang, Y. F., and Rocque, P. A. (1990) Mammalian Thioltransferase (Glutaredoxin) and Protein Disulfide Isomerase Have Dehydroascorbate Reductase-Activity. *J. Biol. Chem.* 265, 15361–15364.
- (160) Cairns, R. A., Harris, I. S., and Mak, T. W. (2011) Regulation of cancer cell metabolism. *Nat. Rev. Cancer* 11, 85–95.
- (161) Vander Heiden, M. G., Cantley, L. C., and Thompson, C. B. (2009) Understanding the Warburg Effect: The Metabolic Requirements of Cell Proliferation. *Science* 324, 1029–1033.
- (162) Krebs, H. A. (1938) Metabolism of amino acids and proteins. *Annu. Rev. Biochem.* 7, 189–210.
- (163) Gallagher, F. A., Kettunen, M. I., Day, S. E., Lerche, M., and Brindle, K. M. (2008) C-13 MR spectroscopy measurements of glutaminase activity in human hepatocellular carcinoma cells using hyperpolarized C-13-labeled glutamine. *Magn. Reson. Med.* 60, 253–257.
- (164) Cabella, C., Karlsson, M., Canape, C., Catanzaro, G., Serra, S. C., Miragoli, L., Poggi, L., Uggeri, F., Venturi, L., Jensen, P. R., Lerche, M. H., and Tedoldi, F. (2013) In vivo and in vitro liver cancer metabolism observed with hyperpolarized [5-C-13]glutamine. *J. Magn. Reson.* 232, 45–52.
- (165) Reynolds, M. R., Lane, A. N., Robertson, B., Kemp, S., Liu, Y., Hill, B. G., Dean, D. C., and Clem, B. F. (2014) Control of glutamine metabolism by the tumor suppressor Rb. *Oncogene* 33, 556–566.
- (166) Gallagher, F. A., Kettunen, M. I., Day, S. E., Hu, D. E., Karlsson, M., Gisselsson, A., Lerche, M. H., and Brindle, K. M. (2011) Detection of Tumor Glutamate Metabolism In Vivo Using C-13 Magnetic Resonance Spectroscopy and Hyperpolarized [1-C-13]-glutamate. *Magn. Reson. Med.* 66, 18–23.
- (167) DeBerardinis, R. J., and Cheng, T. (2010) Q's next: The diverse functions of glutamine in metabolism, cell biology and cancer. *Oncogene* 29, 313–324.
- (168) Dang, L., White, D. W., Gross, S., Bennett, B. D., Bittinger, M. A., Driggers, E. M., Fantin, V. R., Jang, H. G., Jin, S., Keenan, M. C., Marks, K. M., Prins, R. M., Ward, P. S., Yen, K. E., Liau, L. M., Rabinowitz, J. D., Cantley, L. C., Thompson, C. B., Vander Heiden, M. G., and Su, S. M. (2009) Cancer-associated IDH1 mutations produce 2-hydroxyglutarate. *Nature* 462, 739–744.
- (169) Chaumeil, M. M., Larson, P. E. Z., Yoshihara, H. A. I., Danforth, O. M., Vigneron, D. B., Nelson, S. J., Pieper, R. O., Phillips, J. J., and Ronen, S. M. (2013) Non-invasive in vivo assessment of IDH1 mutational status in glioma. *Nat. Commun.* 4, 2429.
- (170) Karlsson, M., Jensen, P. R., in't Zandt, R., Gisselsson, A., Hansson, G., Duus, J. O., Meier, S., and Lerche, M. H. (2010) Imaging of branched chain amino acid metabolism in tumors with hyperpolarized <sup>13</sup>C ketoisocaproate. *Int. J. Cancer* 127, 729–736.
- (171) Marjanska, M., Iltis, I., Shestov, A. A., Deelchand, D. K., Nelson, C., Ugurbil, K., and Henry, P. G. (2010) In vivo C-13 spectroscopy in the rat brain using hyperpolarized [1-C-13]pyruvate and [2-C-13]pyruvate. *J. Magn. Reson.* 206, 210–218.
- (172) Park, J. M., Josan, S., Grafendorfer, T., Yen, Y. F., Hurd, R. E., Spielman, D. M., and Mayer, D. (2013) Measuring mitochondrial metabolism in rat brain in vivo using MR Spectroscopy of hyperpolarized [2-C-13]pyruvate. *NMR Biomed.* 26, 1197–1203.
- (173) Yudkoff, M., Daikhin, Y., Grunstein, L., Nissim, I., Stern, J., Pleasure, D., and Nissim, I. (1996) Astrocyte leucine metabolism: Significance of branched-chain amino acid transamination. *J. Neurochem.* 66, 378–385.
- (174) Hutson, S. M., Lieth, E., and LaNoue, K. F. (2001) Function of leucine in excitatory neurotransmitter metabolism in the central nervous system. *J. Nutr.* 131, 846s–850s.
- (175) Suryawan, A., Hawes, J. W., Harris, R. A., Shimomura, Y., Jenkins, A. E., and Hutson, S. M. (1998) Molecular model of human branched-chain amino acid metabolism. *Am. J. Clin. Nutr.* 68, 72–81.
- (176) Butt, S. A., Sogaard, L. V., Magnusson, P. O., Lauritzen, M. H., Laustsen, C., Akeson, P., and Ardenkjær-Larsen, J. H. (2012) Imaging cerebral 2-ketoisocaproate metabolism with hyperpolarized <sup>13</sup>C magnetic resonance spectroscopic imaging. *J. Cereb. Blood Flow Metab.* 32, 1508–1514.
- (177) Ikonomidou, C., and Turski, L. (1996) Neurodegenerative disorders: Clues from glutamate and energy metabolism. *Crit. Rev. Neurobiol.* 10, 239–263.
- (178) Bowen, S., and Ardenkjær-Larsen, J. H. (2013) Formulation and utilization of choline based samples for dissolution dynamic nuclear polarization. *J. Magn. Reson.* 236, 26–30.
- (179) Lerche, M. H., Jensen, P. R., Karlsson, M., and Meier, S. (2014) NMR Insights into the Inner Workings of Living Cells. *Anal. Chem.*, DOI: 10.1021/ac501467x.
- (180) Bowen, S., and Hilty, C. (2009) Temporal Chemical Shift Correlations in Reactions Studied by Hyperpolarized Nuclear Magnetic Resonance. *Anal. Chem.* 81, 4543–4547.
- (181) Bowen, S., Zeng, H., and Hilty, C. (2008) Chemical shift correlations from hyperpolarized NMR by off-resonance decoupling. *Anal. Chem.* 80, 5794–5798.
- (182) Zeng, H., Bowen, S., and Hilty, C. (2009) Sequentially acquired two-dimensional NMR spectra from hyperpolarized sample. *J. Magn. Reson.* 199, 159–165.
- (183) Zeng, H., Lee, Y., and Hilty, C. (2010) Quantitative Rate Determination by Dynamic Nuclear Polarization Enhanced NMR of a Diels–Alder Reaction. *Anal. Chem.* 82, 8897–8902.
- (184) Bowen, S., and Hilty, C. (2008) Time-Resolved Dynamic Nuclear Polarization Enhanced NMR Spectroscopy. *Angew. Chem., Int. Ed.* 47, 5235–5237.